Agile wheeled mobile robots for service in natural environment

Jean-Christophe FAUROUX
Belhassen-Chedli BOUZGARROU
Nicolas BOUTON
Clermont University, French Institute for Advanced Mechanics (IFMA), EA3867, FR TIMS / CNRS 2856, Mechanical Engineering Research Group (LaMI), BP 10448, F-63000

referencing previous work with:
Philippe VASLIN
Roland LENAIN
Frédéric CHAPELLE

ABSTRACT

Although the wheeled locomotion proved to be very efficient on smooth grounds, it still encounters great difficulties in natural environments, where the ground is subject to wide variations in term of geometry (irregular surface, presence of obstacles...) and material properties (cohesion, grip condition...). This chapter presents recent developments and original systems that allow to model and improve the capacities of wheeled mobile service robots on natural ground.

First is considered the case of low speed motion. Section 2 presents recent results on reconfigurable suspensions that have two states and can decrease lateral friction and energy consumption during turns for skid-steering vehicles. Section 3 presents an original hybrid kinematics that combines wheels with an articulated frame for creating a mobile wheeled robot with high obstacle-climbing capacities, using only one supplemental actuator.

Other advances deals with high speed motion. Section 4 describes a new device dedicated to vehicle dynamic stability, which improves lateral stability on fast mobile robots during turns and contributes to rollover prevention. Finally, Section 5 introduces innovative suspensions with two DOF for fast obstacle crossing. They damp vertical shocks, such as ordinary suspensions, but also horizontal ones, contributing to tip-over prevention on irregular grounds that feature many steep obstacles.

1. INTRODUCTION

Wheeled locomotion still prevails in the 21st century because of high efficiency on various types of grounds, mechanical simplicity and ease of control. In natural environment, though, wheels are challenged by other locomotion modes, such as tracks, that provide excellent grip on low cohesion grounds, or legs, that allow moving on irregular environment and cross obstacles.

This chapter presents recent developments that allow to model and improve the capacities of wheels with additional systems such as innovative suspensions that can have reconfigurable state or additional mobilities. Another interesting solution is to create hybrid systems between wheels and legs, by putting a wheel on a leg or even by transforming the rigid frame of the vehicle into a mechanism.

These new paradigms are particularly interesting in a time where electric actuators can be decentralized close to each wheel, instead of using a central explosion engine, which is still the archetype for most of the cars now. All these solutions appear to be promising and will improve agility of the service robots of the future. Many tasks are becoming possible, such as transport on unstructured grounds and fast inspection by fleets of small agile robots. Civil and military service applications can be imagined for agriculture, forestry, transport, disabled people, industry, defense and crisis management during natural catastrophes.

This chapter is divided in four sections, that can be classified according to speed (Low speed / High speed) or function (Turning / Obstacle-crossing) as shown in Table 1. Here is a summary of section contents:

- Section 2 analyzes the skid-steering process at low speed of a 6x6 wheeled vehicle [Fauroux 04-1, 04-2, 07-1, 10-1]. Skid-steering has similarities with what happens on tracked vehicles: because of transverse friction, a lot of energy is dissipated during steering. This section proposes a model of the vehicle behaviour as well as experimental results, with the general goal to both understand the phenomena and also improve these category of very robust vehicles.
- Section 3 deals with another low speed challenge : obstacle crossing. In this part is introduced OpenWheel i3R, an agile modular mobile robot designed by the authors, with articulated chassis and four motorized wheels [Fauroux 06, 07-2, 08, 09, 10-2, Bouzgarrou 09]. Chassis mobilities are used to maintain the wheel contacts on ground surface and lift off the wheels during cross-over maneuvers in front of obstacles. This maneuver can be seen as a climbing mode which uses both wheels and inter-axle actuation, thus pertaining to the category of hybrid locomotion. After giving a geometric model and the minimal equations for its control, some experimental results are provided, based on the three prototypes created both at small scale (30cm) and high scale (2m).
- Section 4 concerns mainly high speed applications and fast steering, allowing safe control based on dynamic stability. This section presents the development of new devices dedicated to lateral dynamic stability and rollover prevention based on predictive control law and grip conditions observers [Bouton 07-1, 07-2]. Application to fast mobile robots and light all-terrain vehicles are provided.
- Section 5 focuses on another high speed application, this time for obstacle crossing. This section presents a dynamic multibody model of a vehicle crashing at 10m/s on an obstacle as high as one wheel radius. This generally leads to vehicle tip-over. From this observation is inferred a new concept of suspension with two degrees of freedom, that is capable to damp a vertical shock, such as ordinary suspensions, but also a horizontal one, which is compulsory on irregular grounds that feature many steep obstacles [Fauroux 10-3].

Table 1: Topic dispatching of the different chapter sections.

	Low speed	**High speed**
Turning	Section 2: Skid steering at low speed with a 6x6 architecture	Section 4: High speed safe control based on dynamic stability
Obstacle Crossing	Section 3: Agile robots for obstacle crossing at low speed	Section 5: Innovative suspensions with 2 DOF for high speed obstacle crossing

Topic categorization is first made by *speed*. Natural environment is characterized by irregular ground shapes and a great variety of surfaces that are not easy to discriminate. For this reason, the average speed in natural environment is generally lower than the average speed on structured urban or road environments. Quasi-static modelling will be used in the low speed part, and dynamic effects will be neglected. For high speed purpose in off-road context, the challenge is different. Indeed, new phenomena affect the quality of ground contacts, such as sliding, impacts or even complete loss of contact, that may compromise the vehicle or robot stability. Two approaches are considered. The first one is based on active control, that detects the risks of instability and provides rapid correction to keep the vehicle inside its stability domain. The second one reconsiders the mechatronics architecture of the vehicle suspension and provides innovative kinematics for improved capacities. In this case, control should be kept as simple as possible to be fast enough (passive suspension or fast adjustment of simple parameters, such as stiffness or damping coefficient)

The second classification is based on *functions*. On one side, service robots in natural environment have to perform specific functions, such as *obstacle-crossing*, which is a challenge for wheeled vehicles. On the other side, some classical functions of vehicles, such as *steering*, become difficult because of natural environment and require dedicated methods and solutions. Both topics are covered by this chapter, that presents recent advances in designing and modeling the efficient mobile robots of the future.

2. SKID-STEERING AT LOW SPEED WITH A 6X6 ARCHITECTURE

2.1 Steering and skid-steering in existing vehicles

Skid is a phenomenon that appears with every type of ground vehicle when the external forces applied to the vehicle exceed the capabilities of the vehicle-ground interface [Kececi 06]. Skid may be due to longitudinal inertial forces when accelerating/braking or to lateral inertial forces when steering at high speed and low radius. It may also be due to the design of the vehicle.

Skid always appears with tracked vehicles during turns, even if some of them have front steering tracks [Watanabe 95] because the long contact surface of the track with the ground requires a given torque to steer. Conversely, wheels ensure a reduced contact surface on a plane ground: a point contact with toroidal tires such as motorbike tires; a linear contact with cylindrical tires, such as those used for cars. In reality, because of tire deformation, the contact point or contact line becomes a contact patch and a moderate steering torque may be noted. However, wheels give excellent steering capability while maintaining ground contact. For both tracks and wheels, grip strongly depends on the normal force values and distribution [Mokhiamar 06].

The large majority of wheeled vehicles have steering wheels, which can be the front wheels on classical cars; the rear wheels on power lift trucks or lawn mowers [Besselink 03, 04]; all the wheels on some types of mobile robots and sport cars [Shoichi 86]; two front and two rear wheels out of six [FNSS 08] or four front wheels out of eight on military wheeled armoured vehicles [Patria 08] or truck-mounted cranes. The steering mechanism may be complex, particularly when there are more than two steering wheels. The initial constraint is to respect the Ackermann steering geometry (1817), also known as Jeantaud geometry (1851) in Europe, that minimizes skid during low speed turns. This condition requires that all wheels share the same centre of rotation in every position. However, vehicles with more than two axles generally do not completely respect Ackermann geometry (Figure 1). As an example, a semi-trailer does not respect Ackermann geometry and the three fixed rear axles generate severe wear of the tires. The second constraint is that the steering system must be compatible with other functions such as transmission and suspension. This increases mechanical complexity. Another drawback of architectures with steering wheels is that they generally do not allow the rotation of the vehicle on itself (null turning radius). For instance, a four wheel vehicle turning on itself with two steering wheels would require a high steering angle, which is technically complex to design and dangerous at high speeds.

For this reason, many all-terrain vehicles still rely on fixed wheels with no steering mechanism and optional suspensions (Figure 2). These vehicles have a robust and reliable behaviour on rough terrain. Most of them have a 4x4 transmission, such as the Pioneer3-AT robot [Robosoft 09], and some have a 6x6 one, such as multi-purpose amphibian vehicles [OasisLLC 09]. They must turn by skid-steering and behave like tracked vehicles [Mac Laurin 06]. During skid-steering, the wheels that are not tangent to the curved trajectory have to skid laterally, which generates friction forces that oppose to the rotation.

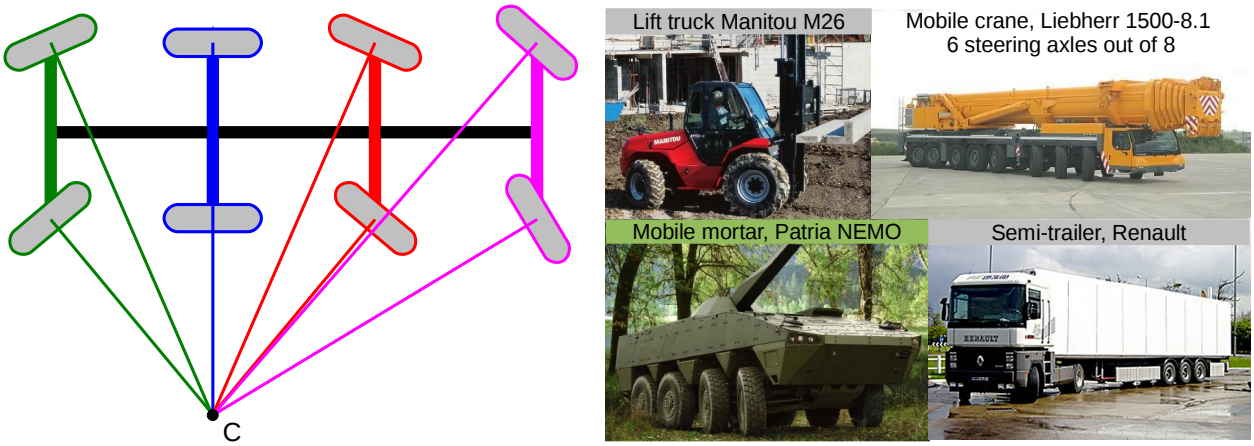

Figure 1: Ackermann steering geometric condition with multiple axles: all the wheels share the same centre of gyration. However, it is rarely completely respected on vehicles with more than two axles.

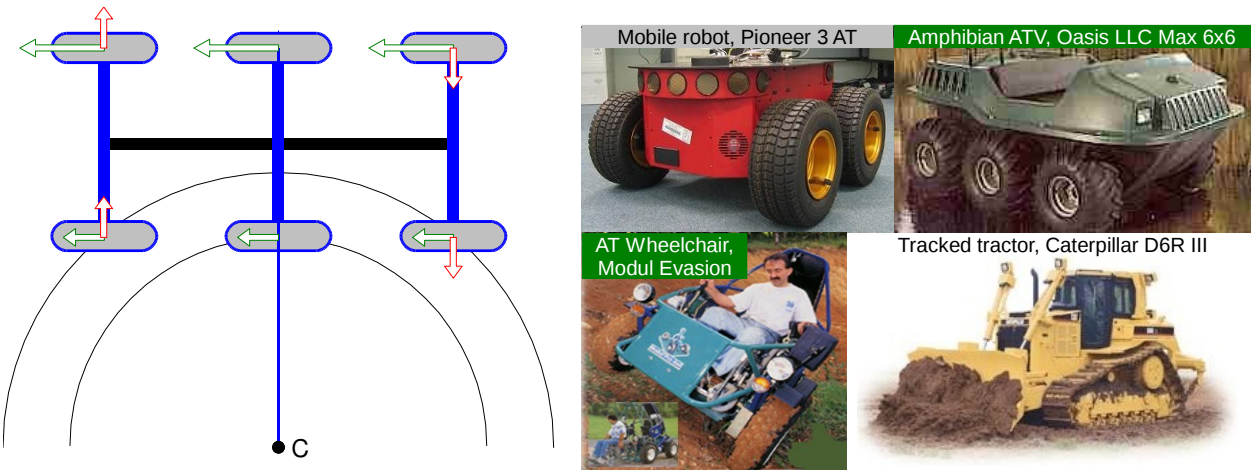

Figure 2: Schematic principle of skid steering with several axles, that generates lateral friction forces. Many all-terrain vehicles and robots do not have steering wheels and behave like tracked vehicles.

The purpose of this work is to model and experiment skid-steering in a 6x6 configuration. This section also explores a solution to reduce energy loss during skid-steering. Although lateral friction is a well-known problem of such types of vehicles with non-directional wheels, it appears that very few studies have tried to reduce lateral friction forces. Most research is focused on the improvement of longitudinal adherence to improve traction and occasionally stability on rough terrain, such as the work on the Gofor Mars exploration robot done by Sreenivasan and Wilcox [Sreenivasan 94]. Reducing steering friction forces could enhance the interest in this class of simple, robust and inexpensive vehicles.

2.2 Description of the 6x6 mobile platform

The Kokoon mobile platform is an all-road 6x6 electric wheelchair [Fauroux 04-1] designed by a group of students of the French Institute for Advanced Mechanics (IFMA) from 1999 onwards (Figure 3).

Kokoon is driven by two direct-current permanent-magnet electric motors of 1330W each (Motovario 24V) and is capable of moving at 8 km/h on 20 % slopes and of climbing easily over 15 cm obstacles. Each motor is controlled by a speed controller (Curtis 1227) that allows current peaks of around 200A from lead-acid batteries. Kokoon is 175 cm long and 103 cm wide and is equipped with six wheels of 20 cm radius with 7 cm wide air-inflated tires (Figure 4a).

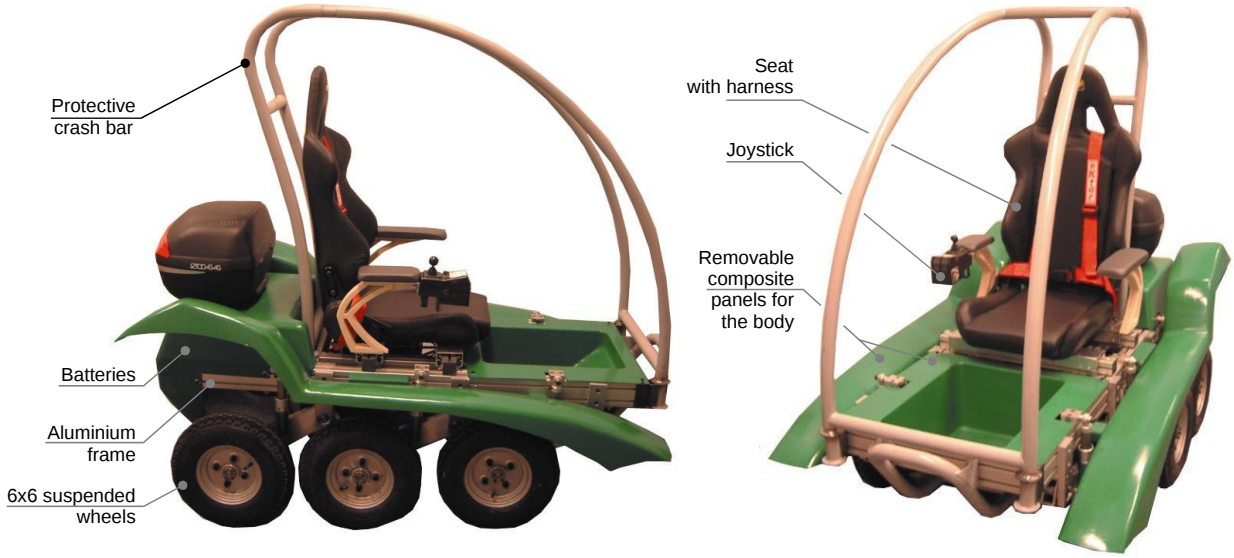

Figure 3: Overview of the 6x6 all-terrain vehicle developed at IFMA since 1999 and named Kokoon.

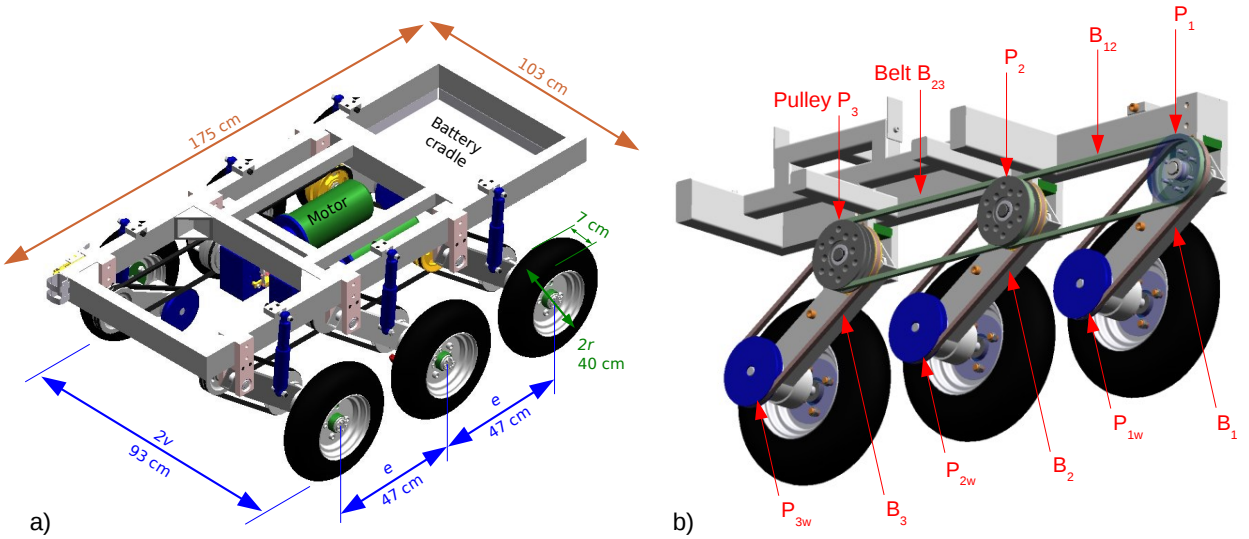

Figure 4: (a) CAD model of the Kokoon frame with its main dimensions.
(b) Left side belt transmission. The electric engine is connected to pulley P_2.

Each motor drives synchronously the 3 wheels of one side thanks to a belt transmission using 6 pulleys and 5 belts (Figure 4b). The motor is directly connected to pulley P_2 by a clutching system (not represented). Belts B_{12} and B_{23} transmit the driving torque to front pulley P_1 and rear pulley P_3 respectively. Pulleys P_i are mounted free and co-axial on swing-arm axes. Belts B_1 , B_2 , B_3 are located on the 3 independent swing arms and drive the power to the last pulleys P_{1w} , P_{2w} , P_{3w} that are linked to the wheels.

The six independent swing arm suspensions use oleo-pneumatic shock absorbers (Figure 5). The top end of the shock absorber is named T and can be longitudinally translated along the T-slots or vertically elevated by spacers. The shock absorbers (Fournales , Inc.) are designed to be inflated at 10 bars using an air pump. Adjusting pressure alters both the pre-constraint and the stiffness. Initially designed for disabled people, Kokoon is an interesting research platform because it has a modular design and can be easily reconfigured [Fauroux 04-2]. Parameters such as transmission, suspension geometry or mass distribution can be adjusted rapidly.

In the field, the Kokoon 6x6 vehicle showed diverse behaviours during skid steering according to the type of ground. On low adherence grounds such as grass or tiled floor, the vehicle could easily turn on itself. But on highly adherent grounds such as tarmac, the vehicle could not steer on itself. In general, low turning radii and and low longitudinal speeds led to difficult steering and high energy consumption. This phenomenon is studied in detail in the following sections and the results obtained below are easily transposable to comparable vehicles and mobile robots with three or more axles.

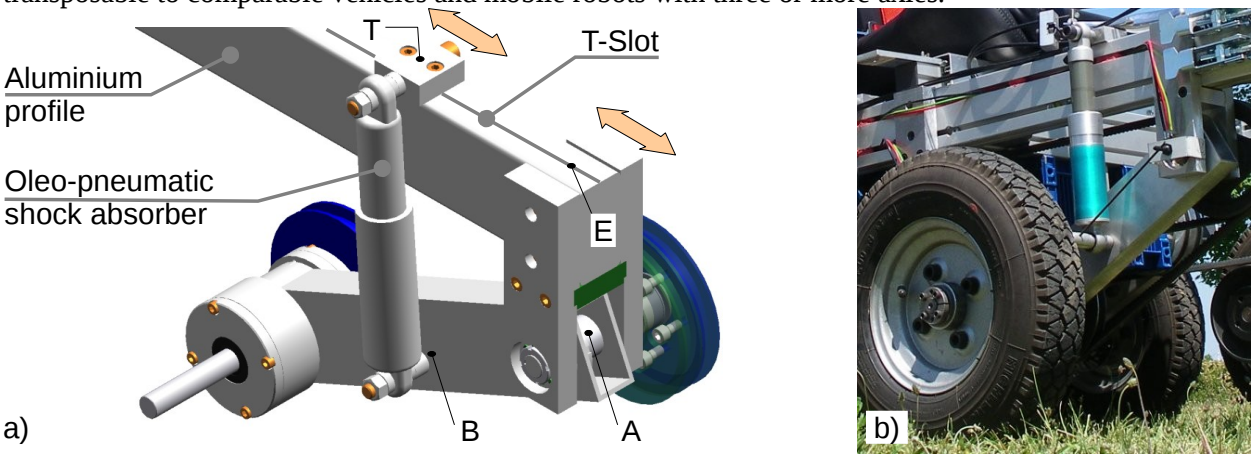

Figure 5: Adjustable swing arm suspension with oleo-pneumatic shock absorber. (a) CAD. (b) Prototype.

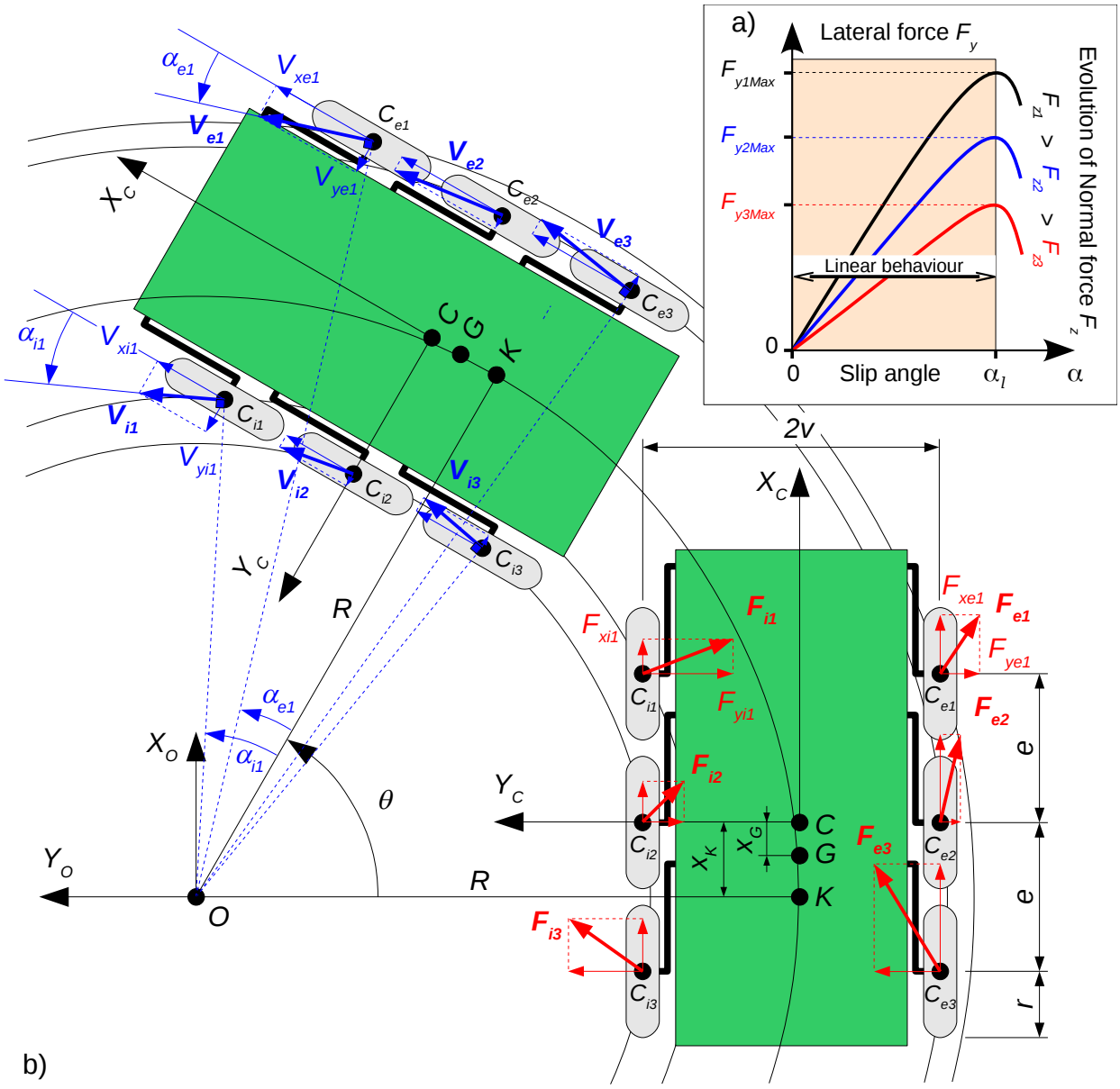

Figure 6: (a) Qualitative graph of the lateral force F_y according to slip angle α and normal force F_z [Halconruy 95]. (b) Top view model of skid-steering with non-symmetrical front and rear slip angles.

2.3 Non-symmetrical skid-steering model

Most vehicles do not have their centre of gravity *G* located at the centre *C* of the lifting polygon (in this case, the centre of the central axle). For this reason, a realistic non-symmetrical skid-steering model has been introduced [Mousset 08]. It is important to keep in mind that the vehicle can turn because of the longitudinal and lateral forces. Longitudinal forces are provided by the engines. Lateral forces result either from lateral accelerations or from friction when skid steering. In this case, the low and rather constant speed used for testing (around 5km/h) allows to neglect the lateral forces resulting from lateral acceleration. This means the lateral forces derive only from friction.

The slip angle α is the angle between the velocity of a wheel contact point and the wheel longitudinal axis (*e.g.* α_{e1} for the external wheel of axle 1 on the Figure 6b). The relation between the lateral force F_y and the corresponding slip angle α is quasi-linear up to a limit value α_l, as represented in Figure 6a [Halconruy 95]. The angle α_l is of the order of 10° for a typical car tire.

Above this threshold, there is a transition zone and the tire starts to slip on the ground. So with identical front and rear slip angles, the vehicle should be submitted to equivalent front and rear lateral forces and the front and rear slip angles should remain equal throughout the whole process. But Figure 6a also shows that the lateral force F_y depends on the normal force F_z: an increase of F_z generates an increase of F_y. With a non-balanced vehicle, the load on each axle is no longer identical and the slip angles vary accordingly. For instance, a turning vehicle that is heavier on axle 3 has an increased slip angle and lateral force on the rear and the global dynamic equilibrium is altered.

Figure 6b represents the non-symmetrical model of a vehicle with the centre of gravity at the rear. Two positions are shown corresponding to a rotation of angle θ and radius *R* around centre *O*. Forces are drawn on the right position while speeds are represented on the top position. Amplitudes and directions of forces $\boldsymbol{F_{sa}}$ and speeds $\boldsymbol{V_{sa}}$ are represented qualitatively for wheels of side *s* (that can be *e* for external or *i* for internal) and axle *a* (that can be 1 for front, 2 for middle or 3 for rear axle) respectively. All forces and speeds are applied at wheel-centres, denoted C_{sa}. Point *G* is the vehicle centre of gravity. Point *C* is the geometric centre of the lifting polygon. Point *K* is defined as the orthogonal projection of the gyration centre *O* into the sagittal plane (C, X_C, Z_C). On the right of Figure 6b, the different reaction forces of the ground to the vehicle are represented by vectors $\boldsymbol{F_{sa}}$, applied on side *s* and axle *a*. The forces $\boldsymbol{F_{sa}}$ have a longitudinal component F_{xsa} which is the longitudinal reaction of the ground to the vehicle propulsion force applied by the engine and are not know individually but obey to equations (1):

$$F_{xe1}+F_{xe2}+F_{xe3}=\frac{\tau_e}{r} \qquad F_{xi1}+F_{xi2}+F_{xi3}=\frac{\tau_i}{r} \tag{1}$$

where τ_e and τ_i are the torques of the motors of the external and internal wheels respectively and *r* is the wheel radius. The reaction forces $\boldsymbol{F_{sa}}$ also have a lateral component F_{ysa} which is the ground reaction force opposed to the transversal slipping of the tire, generated because of slip angles.

In Figure 6b, the speeds $\boldsymbol{V_{sa}}$ are represented on the top position of the vehicle with a magnitude that is proportional to the distance between *O* and the considered wheel-centre C_{sa}. Generally, this means external wheels turn faster than internal ones. Even on the same side, each wheel-centre C_{sa} moves around a separate circle. The speed vectors $\boldsymbol{V_{sa}}$ are constructed tangent to the circular trajectory of C_{sa}, with two components: the longitudinal speeds V_{xsa} are oriented to the front of the vehicle; the lateral speeds are denoted V_{ysa}. Each time V_{ysa} is non null, there is lateral slipping of the wheel which generates a lateral force in the opposite direction.

The slip angles α_{sa} are obtained via equation (2) as a function of x_a which is the longitudinal distance between axle *a* and the projected gyration point *K*. The value of x_a depends on the wheelbase *e* and on the longitudinal position x_K of point K relative to (C, X_C), which is negative in Figure 6.

$$\alpha_{ea}=atan\left(\frac{x_a}{R+v}\right) \qquad \alpha_{ia}=atan\left(\frac{x_a}{R-v}\right) \text{ with } x_a\in\left\{e-x_K,-x_K,-e-x_K\right\} \tag{2}$$

Assuming that the skid-steering vehicle has a constant rotation speed, the fundamental principle of dynamics can be applied with a null rotational acceleration around axis (O, Z_O). If the friction in the transmission is initially ignored, it can be interpreted in the following way: the steering torque generated by the longitudinal forces created by the motors is used to compensate exactly for the resisting torque created by the slipping lateral forces. This results in equations (3)-(4).

$$M_{O,F_{xsa}}+M_{O,F_{ysa}}=0 \tag{3}$$

$$\left(\sum_{a=1}^{a=3}F_{xea}.(R+v)+\sum_{a=1}^{a=3}F_{xia}.(R-v)\right)+\left(\sum_{a=1}^{a=3}(F_{yea}+F_{yia}).x_a\right)=0 \text{ with } x_a\in\left\{e-x_K,-x_K,-e-x_K\right\} \tag{4}$$

Equation (1) allows to replace longitudinal forces by motor torques and to obtain:

$$\left(\tau_e.\frac{(R+v)}{r}+\tau_i.\frac{(R-v)}{r}\right)+\left(\sum_{a=1}^{a=3}(F_{yea}+F_{yia}).x_a\right)=0 \text{ with } x_a\in\left\{e-x_K,-x_K,-e-x_K\right\} \tag{5}$$

Equation (5) governs the skid-steering behaviour and may help to characterize it, provided that sufficient data are gathered from experiments. In the next subsection, we present an original solution to reduce the friction forces F_{ysa} during skid-steering. By decreasing the absolute value of the second term in Equation (5), that represents the skid-steering resisting torque, it appears that the driving torque represented by the first term will simultaneously decrease as an absolute value. This could be an advantageous improvement on this class of vehicles.

2.4 Reconfiguring the suspensions to modify the contact forces

The lateral friction forces F_{ysa} are directly proportional to the normal forces F_{zsa} , that depend directly on the mass repartition of the vehicle. The main idea of this work is to adjust the mass distribution by modifying the vehicle suspensions and providing them two different configurations.

For reasons of simplicity, the modification consisted in translating the top-attachment points denoted *T* (Figure 5a) of the front and rear shock absorbers in their T-slot. In the standard configuration, the shock absorbers were vertical at equilibrium (Figure 7a). In the modified configuration (Figure 7b), *T* was translated forward of 100mm for the front and rear shock absorbers. This had two consequences:

- the unloaded altitude of the centre of the front and rear wheels increased
- the average stiffness of the front and rear suspensions decreased.

Because of both simultaneous changes, the vertical forces F_{za} on the front and rear wheels were noticeably lowered. As a consequence, the central axle was strongly overloaded and the central shock absorber underwent visible compression (Figure 7b).

This suspension adjustment is equivalent to change mass distribution, as summarized in Table 2 and demonstrated in [Fauroux 10-1]. The values have been determined independently by three different methods with consistent results: CAD model, direct measurement on scales and experimental measurements on a force-plate.

Table 2: Effects of suspension adjustments on the equivalent mass distribution (including an 83kg driver).

	Front axle (kg)	**Middle axle** (kg)	**Rear axle** (kg)	**Total** (kg)
Standard configuration	108	158	183	450
Modified configuration	80 (-26%)	250 (+58%)	120 (-34%)	450

Front and rear axles were off-loaded by 26% and 34% respectively whereas middle axle loaded 58% more. Adjusting the suspensions was an extremely interesting option because of the small amount of work required and the significant changes generated. The following subsection will now present the real experiments with standard and modified suspensions.

2.5 Experimental results for the standard and modified suspensions

The steering process of a vehicle is a complex phenomenon that may be better understood from an experimental preliminary approach [Itoh 95, Foster 06]. For this 6x6 vehicle, it was decided to measure experimentally the contact forces of the wheels on the ground by rolling on the top plate of a six-component force-plate (TSR, Mérignac, France), rigidly fixed in a wooden box buried in the ground so that the top plate is at ground level [Fauroux 07-1]. The force-plate used in this study was 80 cm long, 60 cm wide and had the following measurement ranges: R_x = 1000 N, R_y = 900 N, R_z = 2000 N with a resolution of 10 N [Couétard 96, 00].

The experimental field can be seen in Figure 7c. Lines showing the desired trajectories across the force-plate were drawn on the ground using flour. Three types of trajectories have been considered in this study: a straight line (which is equivalent to a turn with infinite radius); a turn with a 6 m radius; and a turn with a 3 m radius. Several experiments were performed with the aim of following as closely as possible the desired trajectories.

Figure 8 shows the typical reaction forces applied to the vehicle when it drives over the platform. Because the vehicle wheelbase (47 cm) is smaller than the force-plate width along the rolling direction (60 cm), sometimes only one and sometimes two wheels may be on the force-plate at the same time. This

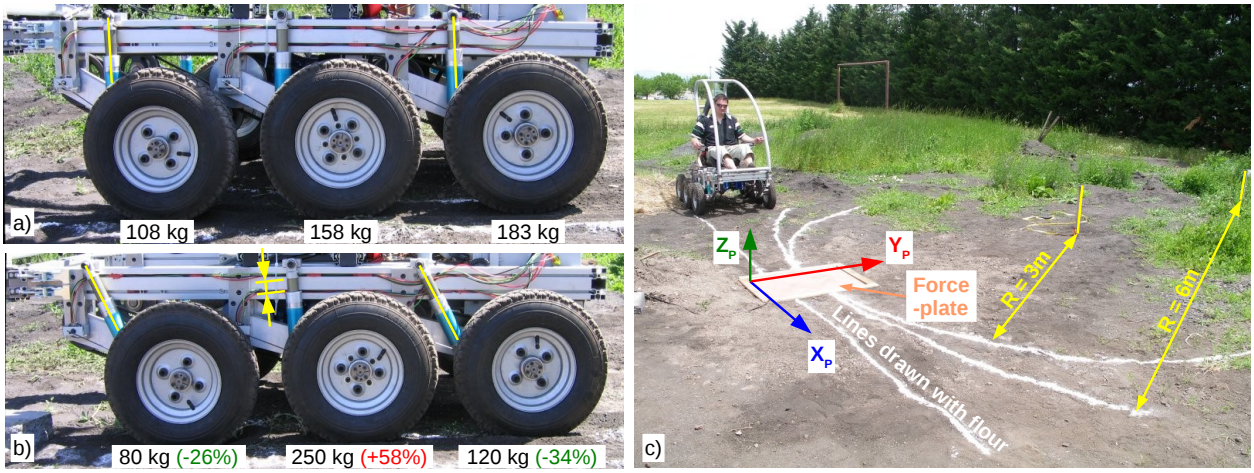

Figure 7: (a) Standard suspension configuration. (b) Modified configuration after adjustment. (c) Experimental contact force measurement with a force-plate along trajectories.

explains the shape of the curves of the reaction forces applied to the vehicle when it crossed the force-plate. The time axis of each trial can be divided into five intervals:

1. First, only wheel 1 applies efforts on the force-plate;
2. Then wheel 2 climbs onto the force-plate (left transparent area) and the vertical component of reaction force R_z increases suddenly;
3. After that, wheel 1 leaves the force-plate and only wheel 2 remains on it;
4. Then, it is up to wheel 3 to cross the force-plate (right transparent area) and a second peak on R_z appears;
5. Finally, wheel 2 leaves the force-plate and only wheel 3 remains on it until the end of the crossing.

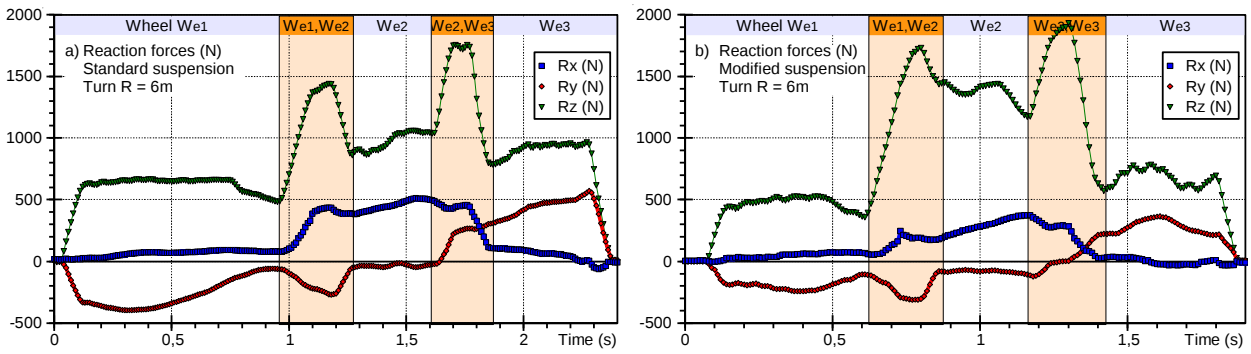

Figure 8: Reaction forces when the 6x6 vehicle drives over the force-plate with R=6m. (a) Standard suspension. (b) Modified suspension. Depending on the time, either 1 or 2 wheels push on the force-plate.

Experiments were made with both the standard (Table 3) and modified (Table 4) configurations of suspensions. The force values are obtained by averaging the R_x , R_y , R_z components on the single wheel intervals and give an order of magnitude of the reaction components, thus eliminating the small variations in the signal due to electrical perturbations and vehicle vibrations on small pieces of gravel.

Results with standard suspension: For normal force R_z in standard configuration, it can be seen in Table 3 that wheel 3 (930 N) bears more weight than wheel 2 (848 N), which, in turn, bears more weight than wheel 1 (635 N). These results include the driver's weight and confirm the previous calculations of the centre of gravity. Assuming that the grip coefficient is identical on every wheel, this means that the rear and central wheels apply a higher propulsion force R_x and may undergo a higher lateral force R_y .

Table 3: Average forces on the right wheels for standard suspensions.

Standard suspensions	Wheel 1 (Front)			Wheel 2 (Middle)			Wheel 3 (Rear)		
	R_X (N)	R_Y (N)	R_Z (N)	R_X (N)	R_Y (N)	R_Z (N)	R_X (N)	R_Y (N)	R_Z (N)
Straight line	23	10	635	-17	-67	848	-30	-40	930
Turn R = 6m	70	-270	627	454	-36	972	68	438	905
Turn R = 3m	74	-321	534	553	-146	1016	86	532	914

Table 4: Average forces on the right wheels for modified suspensions.

Adjusted suspensions	Wheel 1 (Front)			Wheel 2 (Middle)			Wheel 3 (Rear)		
	R_X (N)	R_Y (N)	R_Z (N)	R_X (N)	R_Y (N)	R_Z (N)	R_X (N)	R_Y (N)	R_Z (N)
Straight line	69	-105	446	-155	-33	1393	-43	-95	671
Turn R = 6m	49	-194	468	282	-80	1382	3	281	671
Turn R = 3m	8	-331	563	450	49	1533	-55	398	666

Another interesting result is the evolution of R_x with respect to the steering radius R: when R decreases, R_x must increase to make the vehicle rotate, as expected from Equation (4). Along a straight line, R_x does not need to be very high in order to generate vehicle movement. But during a turn with R = 6 m (respectively 3 m), R_x on wheel 2 reaches 454 N (resp. 553 N). This increase in R_x force was clearly experienced by the driver, who needed to increase the power during short turns.

As expected, the lateral force R_y has a negligible value when driving in a straight line. However, this value increases particularly on the front and rear wheels when the turning radius R decreases. For instance, for the 3 m turn, R_y reaches -321 N (resp. 532 N) on wheel 1 (resp. wheel 3). The opposite signs of R_y between wheels 1 and 3 logically reflect the opposite lateral efforts applied on these wheels during the turn. The absolute values of R_y are not symmetrical on front and rear wheels. One explanation is that axle 3 loads more weight than axle 1. This is also the case for the 3 m turn, where R_y is non null on wheel 2 (-146 N). These results seem to confirm that the centre of gyration of the vehicle is not located on the central axle, as predicted by the non-symmetrical skid-steering model presented in section 2.3.

Results for the modified configuration of suspensions: The results are summarized in Table 4. For a 6 m turn with the modified vehicle, the lateral force R_y decreased of 28% on the front axle and 36% on the rear axle. This means that less energy was dissipated during skid-steering with the modified suspensions.

With modified suspensions, measurements clearly showed the the important part of the vertical load borne by wheel 2 (Figure 9b) with respect to the original configuration (Figure 9a).

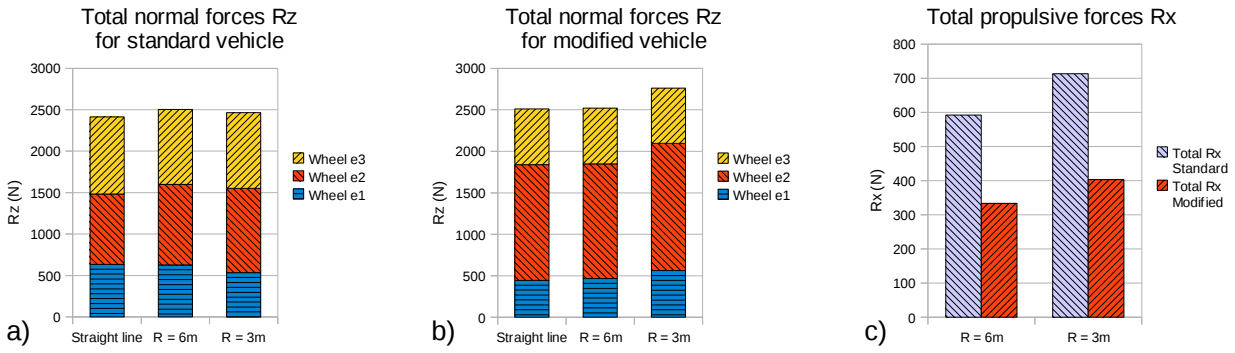

Figure 9: Total of forces for external wheels. (a) Normal forces R_z for standard suspensions. (b) R_z for modified suspensions. (c) Total propulsive forces R_x for standard and modified suspensions.

The modified suspension also seems to have decreased the required propulsion force. This could mean that a smaller longitudinal force was able to generate the same movement of the vehicle. For a 6 m turn, R_x decreased from 454 N to 282 N on the central wheel (Table 3 and 4), which means a gain of 38% with respect to the initial suspension adjustment. The decrease of the sum of the propulsive forces R_x of all the external wheels is also visible in Figure 9c. The force decrease is quantified at 43.5%, for radius 6 m as well as 3 m. The overall turning time was observed to be shorter than with a classical suspension and the driver needed to inject less energy into the electric motors. This suggests that the global turning efficiency was improved with the modified suspension.

2.6 Conclusion on reconfigurable suspensions for skid-steering

This work has presented models and experiments of the skid-steering phenomenon on a 6x6 vehicle. It characterized the lateral skid forces that are responsible for a high level of energy dissipation during steering. It also showed that the projected centre of gyration *K* depends on the vehicle mass distribution as well as its propulsion and suspension systems. Experimental results seem to confirm that point *K* is not located on the central axle of the vehicle, which corroborates the proposed non-symmetrical skid-steering model. Further work based on the simultaneous measurement of contact forces using integrated 6-component force sensors on every wheels will locate point *K* precisely for a better skid-steering control.

This work also showed that a small adjustment in the suspensions may allow a substantial decrease of 40% of the propulsion forces during skid-steering. Indeed, on vehicles with three or more axles, one can imagine an adaptive suspension capable of modifying the normal force distribution on the wheels without changing neither mass nor payload distribution in the vehicle. In the next version of our Kokoon vehicle, the suspension adjustment will be automatically performed only during turns by using an active mechanism, resulting in lower energy consumption during skid-steering. When driving in a straight line, the adjusting mechanism would reset the initial normal force distribution for better balancing of traction forces on all the axles together with improved pitch stability. This would combine the robustness of swing-arm suspensions without the drawback of energy consumption during skid-steering.

3. Agile robots for obstacle crossing at low speed

This section presents the elaboration of an innovative principle for climbing obstacles within the framework of an open architecture for designing wheeled robots, keeping the efficiency of the wheels while improving mobility and static stability by a good compromise between climbing performance, complexity, stiffness and technological pragmatism. This last point includes a reasonable number of wheels and actuators. The application field of the climbing method and paradigms described here is located at the interface between commercial wheeled vehicles and mobile robots with original kinematics.

3.1 Steering and skid-steering in existing vehicles

Vehicles are considered as systems driven by their own propulsion device and intended to move people and payloads in an outside environment, most of the time controlled by a human operator. Usual applications may be transport, agriculture or leisure. Mobile robots have a higher degree of autonomy and are more specially designed to challenge with complex reproducible tasks. For this aim, they usually have reactive behaviour with the help of sensors for internal and external perception, actuators, control laws and strategies for interpretation of sensory data and decision [Devy 95]. They are usually intended to exploration or inspection tasks, often at low speed. The mechanical architecture can allow mono or multi-modes of locomotion. Most of the time, all the wheels are motorised. Mobile robots differ with chassis internal mobilities, than can be passive (without actuators) or include some actuated mobilities (active robots). Additional sensors allow to adapt to unknown factors and ground changes (reactive robots).

The wheeled terrestrial propulsion is known to be a very energy-efficient way of moving, because energy is mainly used for propulsion and not lift [Bekker 69]. Wheels are particularly fast on flat grounds but have difficulties to deal with obstacles and terrain discontinuities. Climbing obstacles remains a challenge for these systems. Qualities such as low power consumption, reliability and adaptability to the ground insuring a good locomotion are no more guaranteed. In that case, legged type of locomotion

regains interest (discrete discontinuous ground contacts). It needs complex control and require high energy for high speed. Several robots offer a hybrid architecture by mounting wheels on/with legs, e.g. [Grand 04, Halme 03, Hirose 96, Nakajima 04], combining more than two locomotion types [Michaud 03], climbing by hopping [Kikuchi 08], or presenting original articulated frames [Apostolopoulos 01, Lacroix 02, Rollins 98] in order to locate and orientate wheels for specific purposes. Those special mobile robots generally focus on improving mobility, stability or climbing capabilities. However, this improvement is often obtained at the price of higher complexity, great number of joints, low stiffness and great number of wheels.

All these previous considerations also allow to think that there is enough room for generic and modular mechanical architectures, possibly close to commercial vehicles, developed from new climbing strategies with very slightly actuated frame. Focus is particularly set on new displacements for climbing over obstacles and terrain discontinuities while ensuring static stability. Wheeled locomotion, a mode not really present in nature, should be developed even more towards all-terrain locomotion.

The section introduces a modular architecture for mobile robots and the associated climbing mode making possible to obtain high climbing capacities, with low actuation and good stiffness. The concepts remain sufficiently generic to be easily transposable on existing wheeled vehicles systems (e.g. All Terrain Vehicles (ATV) or quad bikes). The global motorization is chosen to be distributed on the wheels, with one electric motor attached to each wheel, for compactness and genericness. Only one internal supplemental motor will be located at the centre of the frame as described in the following subsections, presenting the paradigm (§3.2) and kinematics (§3.3) of our OpenWHEEL i3R robot. Then are introduced the climbing strategy (§3.4), reduced models(§3.5), full-scale demonstrator(§3.6) and the geometric model used to control and improve the obstacle climbing strategy (§3.7).

3.2 OpenWHEEL paradigm

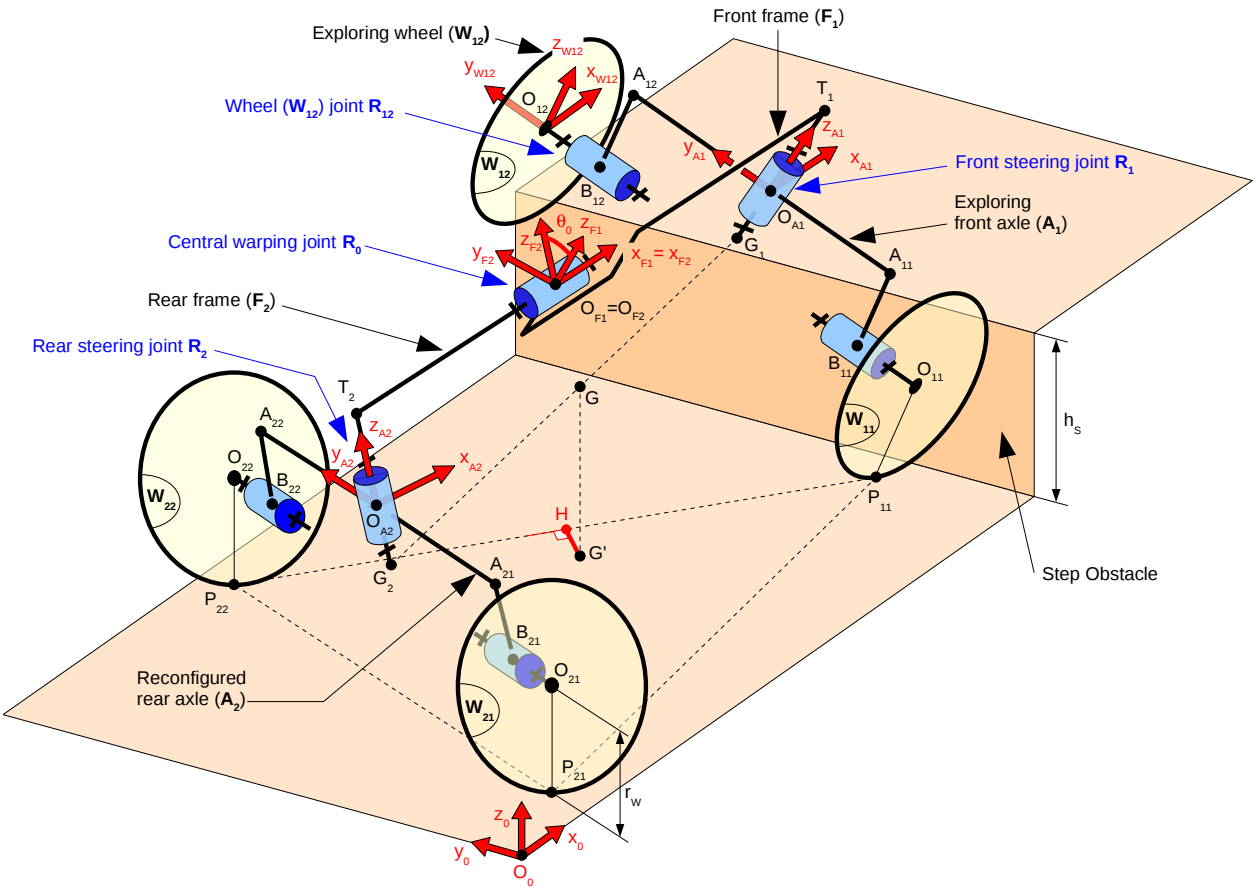

Figure 10: Kinematic structure of OpenWHEEL i3R [Fauroux 09].

OpenWHEEL is the name given to a family of rovers with articulated frame and/or innovative suspensions. The name “i3R” defines its kinematics: “i” for inter-axle, highlighting the central mechanism joining the axles; “3R” for the number of revolute joints present in the robot: one passive steering rotation per axle and one central active warping joint. This kinematics combines the speed of wheeled propulsion with the agility offered by an articulated chassis for good all-terrain performance. Kinematics of OpenWHEEL i3R was first defined in [Fauroux 06]. It features an articulated frame allowing the rover to climb on obstacles and a small number of wheels (4 wheels = 3 wheels for stability + 1 exploring wheel).

A sequential motion strategy was jointly developed to cross an obstacle with a step-profile. The kinematics and strategy are crafted to be "kept as simple as possible", while remaining within the limits of static stability. They were designed to be easy to transfer to a commercial vehicle such as a quad bike or ATV for transport tasks or semi-autonomous inspection, in a spirit of robustness and reliability, notably for the possibility of bearing payload on the field. OpenWHEEL is likely to meet a variety of obstacles. The steepest possible obstacle to find in the external environment is a step-like obstacle. The motion strategy is built with the assumption that the horizontal length of this step is sufficient to permit the robot to stand on top of it on its four wheels. Staircaise climbing [Gonzales 09] is not considered yet but the robot is capable to cross a hurdle (i.e. a thin and high obstacle) using modified movements.

3.3 OpenWHEEL kinematics

The kinematic structure of OpenWHEEL i3R is shown in Fig. 10. The robot is made of two axles named (A_a) with *a* the axle number (1 for front, 2 for rear). Wheels are numbered (W_{as}) with *s* the side number (1 for right, 2 for left). The axles are linked by a serial inter-axle mechanism made of two frames (F_1) and (F_2) connected by three revolute joints R_k and thus named i3R ('i' standing for “inter-axle”).

The central joint R_0 is actuated for the warping of the structure. The R_1 and R_2 joints are passive and are used for dual Ackermann steering. They also give a longitudinal mobility that allows to bring the exploring wheel on top of the obstacle (i.e. wheel W_{12} on Fig. 10). Analysis showed that the robot has a mobility of 3 while rolling and 4 while climbing [Bouzgarrou 09]. Stability is ensured when the projected centre of mass *G'* lays inside the lifting triangle ($P_{11}P_{21}P_{22}$ in Fig. 10). Distance *HG'* gives a geometric representation of the stability margin.

Each link *(L)* of the robot has a local reference frame R_L (O_L, x_L, y_L, z_L). The origins O_{F1} and O_{F2} of the links (F_1) and (F_2) are defined confounded and R_{F1} represent the reference frame of the whole robot. The angles α, β, γ represent respectively the yaw, pitch and roll of frame R_{F1} with respect to ground reference R_0. Angles θ_0 , θ_1 , θ_2 measure respectively the frame warping and axle steering of (A_1) / (A_2). They are defined by: $\theta_0=(\widehat{y_{F1},y_{F2}})=(\widehat{z_{F1},z_{F2}})$, $\theta_1=(\widehat{x_{F1},x_{A1}})=(\widehat{y_{F1},y_{A1}})$ and $\theta_2=(\widehat{x_{F2},x_{A2}})=(\widehat{y_{F2},y_{A2}})$ Only θ_0 is actuated. The steering angles θ_a are indirectly controlled via the self-rotation θ_{as} of the actuated wheels, with $\theta_{as}=(\widehat{x_{Was},x_{Aa}})=(\widehat{z_{Was},z_{Aa}})$. The centre of mass of axle (A_a) is denoted G_a and supposed located on line (O_{Aa}, z_{Aa}), at the middle of the axle (axles are laterally equilibrated).

3.4 OpenWHEEL climbing strategy

The climbing process is a sequence of stages that connect successive characteristic poses of the robot. All the poses are statically stable, *i.e.* when a wheel is lifted, the projection of the centre of gravity is kept within the support triangle formed by the three other wheels. A sequence of 19 stages was first presented in [Fauroux 06] and interpolated to obtain a complete climbing process with quasi-static stability.

In order to climb the obstacle, each wheel has to become successively the “exploring wheel”, being lifted over the obstacle while the robot lays only on three contact points P_{as}. Before lifting the exploring wheel (W_{as}), the robot must be controlled in such a way that the wheel $(W_{a's})$ of the same side *s* but of the other axle *a'* is brought as close as possible to (W_{as}). This allows to maintain *G* strictly above the triangular lifting polygon and to guarantee stability. The robot motion during climbing is described qualitatively in Fig. 11 and the stability margin *HG'* of Fig. 10 is approximated here in 2D in the top view.

The process is divided into 7 phases and 19 stages. Phase A brings the vehicle against the obstacle. Phase B is for (W_{11}) climbing. It is decomposed into 4 stages: stage 2 where the robot reconfigures the

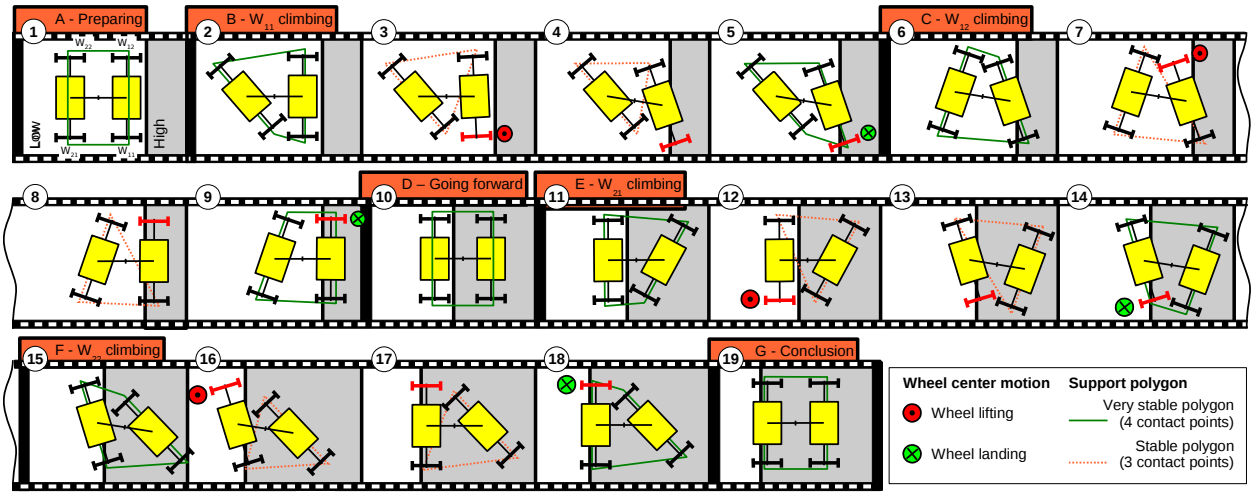

Figure 11: Climbing process of OpenWHEEL i3R in 19 stages.

rear axle *(A2)* to bring *(W21)* close to *(W11)*; stage 3 where *(W11)* is lifted via θ_0 warping; stage 4 where *(W11)* is pushed forward by the rear axle *(A2)*; stage 5 where (*W11*) lands on top of the obstacle via θ_0 unwarping. Phase C unrolls the same process for *(W12)*. Phase D brings the second axle in contact with the obstacle. Similarly, phase E and F are for *(W21)* and *(W22)* respectively. The final F phase serves only to unsteer θ_1 and θ_2. The whole procedure was validated first by an Adams 3D multi-body model [Fauroux 06] and by several demonstrators.

3.5 Small-scale demonstrators

Built from Lego Mindstorms RCX elements, the first model, denoted V1 (Fig. 12) uses a rough open loop control to highlight a number of critical points on certain stages of the crossing [Fauroux 08].

The most critical point is that the tilting of the model may compromise obstacle crossing (Fig. 13). Tilting a vehicle of angle β with a high centre of gravity *G* shifts backward the position of the projected centre of gravity *G'* and induces instability in stages 12 and 16 during climbing of the rear axle. Distance P_2G' is given by equation (6) with b being the wheelbase length and h_l the leg length.

$$P_2G' = b\cos(\beta)/2 - h_l\sin(\beta) \qquad (6)$$

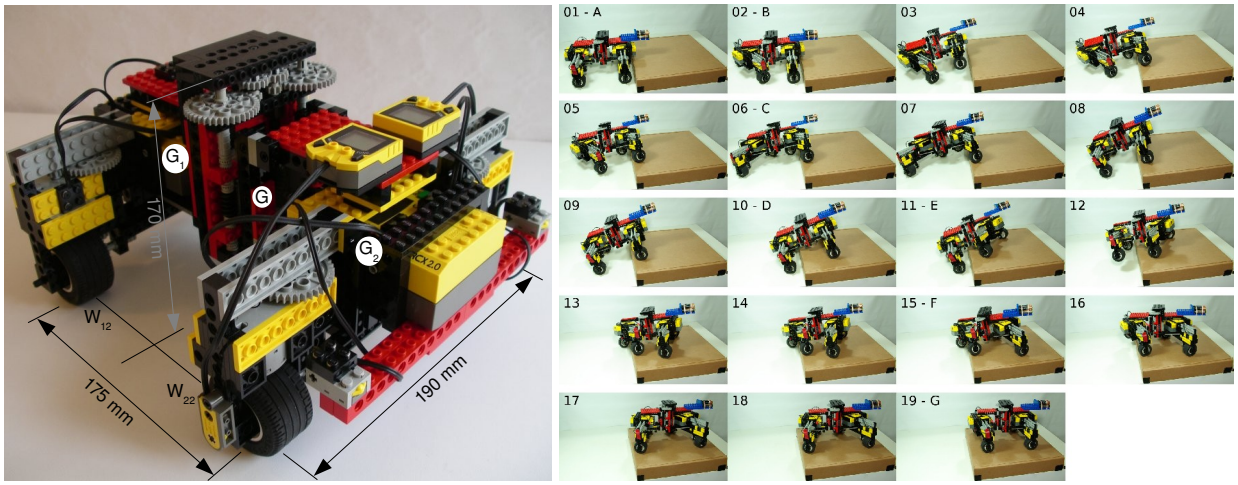

Figure 12: (a) Small scale version of OpenWHEEL i3R V1 with RCX kit. (b) Climbing process.

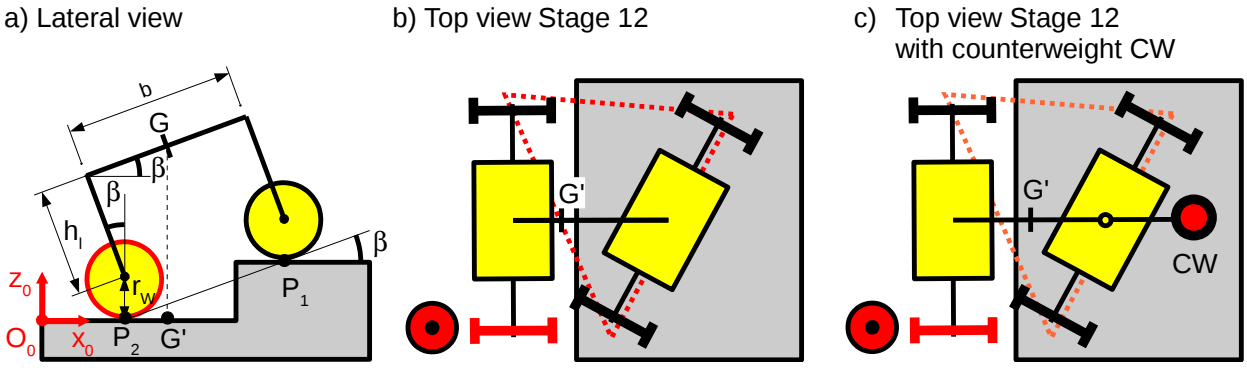

Figure 13: Obstacle crossing is compromised by tilting angle β and restored by a new mass repartition.

The robot seems temporarily heavier from the rear. This phenomenon was analysed in [Fauroux 09] and required the installation of a frontal counterweight CW (Fig. 13c). A qualitative analysis showed that a counterweight of 144g with a robot mass of 1530g, located 90mm forward of G_1 allowed to bring G forward of 16mm (9% of the wheelbase length b = 175mm) and cured the instability.

The second noticeable phenomenon is named steering-warping coupling. It was solved by a corrective modification of control and requires a formalized model that will be presented in §3.7. The last phenomenon is the loss of contact adherence when the normal force decreases or where the obstacle blocks the advance of a wheel, and can be avoided by control adjustments or supplemental force sensors.

Model V1 climbs obstacles of 55mm (Fig. 12b), which seems to be close to the maximum performance for this particular implementation of the robot. The maximum obstacle height does not depend on the wheel diameter and represents 66% of the height of its centre of gravity, which is the metrics we recommend to quantify crossing performance.

A second small scale model, named V2, was based on the Mindstorms NXT next generation kit (Fig. 14). With actuators that include a coder, V2 allowed to test some control laws with closed loops using the NXC programming language, a C like language including a complete NXT API [Hansen 10]. The V2 model has stronger actuators and smaller reduction ratios than V1, which ensures higher dynamics, but still lacks of rigidity. Several sensors where added in V2, such as steering rotation sensors to measure θ_1 and θ_2, distance ultrasound sensors to measure horizontal distance and height of the obstacle, contact sensors on the front to start the climbing process and a 3D accelerometer used as an inclinometer to measure the tilt angle. The NXT control program was designed for V2 and to be be directly implanted on the full-scale demonstrator with only scale constant adjustments.

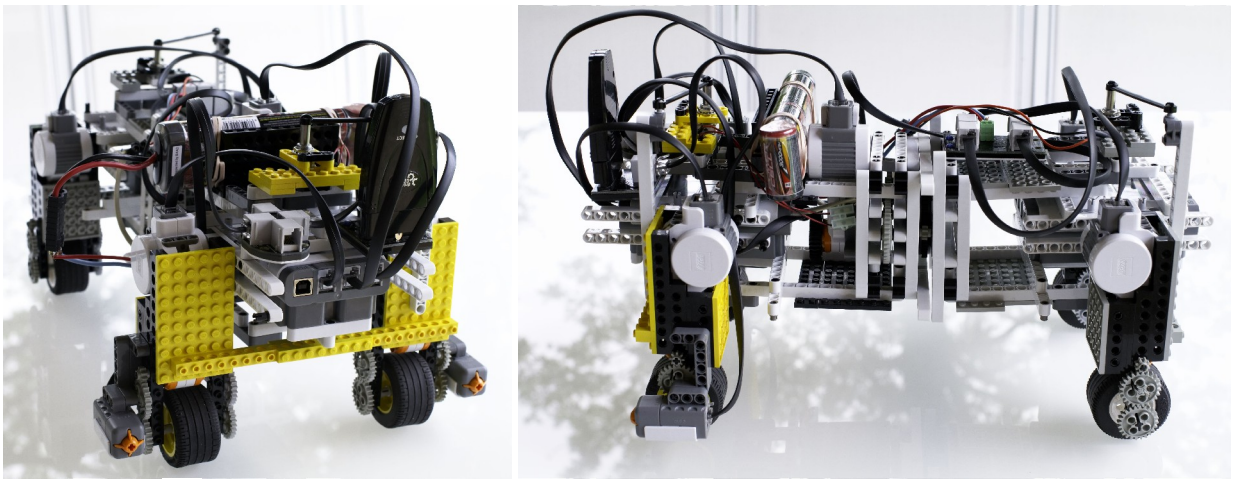

Figure 14: Small scale version of OpenWHEEL i3R V2 with NXT kit and advanced control.

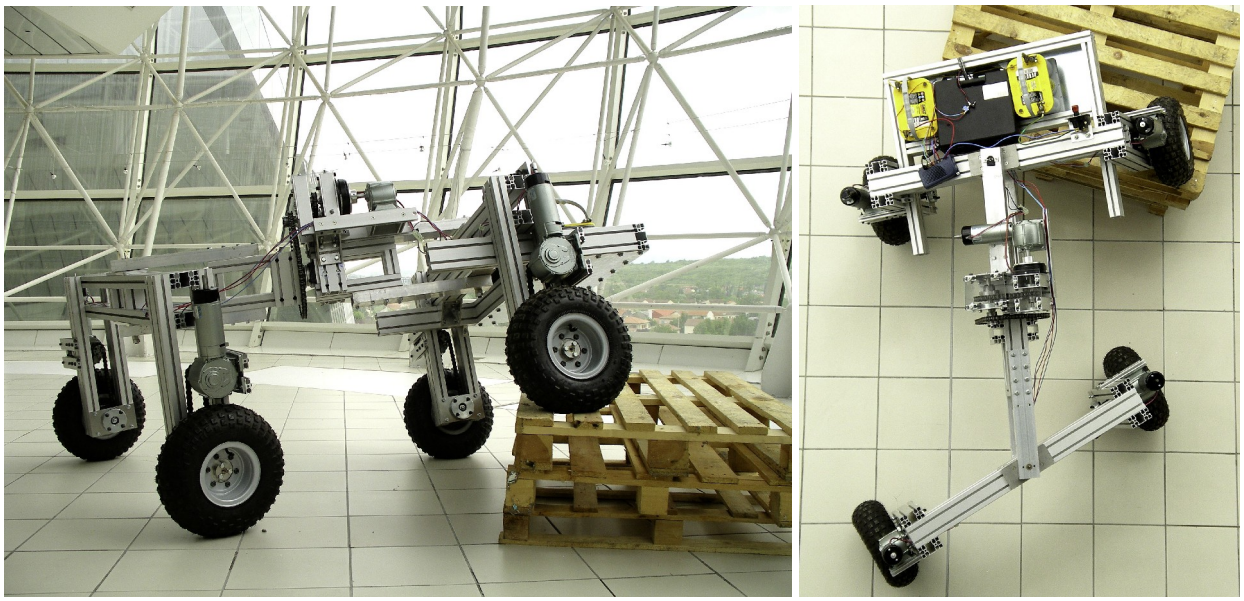

Figure 15: Full-scale OpenWHEEL i3R V3 crossing an obstacle in lateral (a) and top view (b).

3.6 Full-scale demonstrator

The full scale OpenWHEEL i3R V3 robot is around 1.85m long, 1.38m wide, 0.98m high with a total weight approaching 200kg. The robot frame is made of modular aluminium profile. The five identical 24V DC actuators include a coder and have a power of 330W each, a nominal torque of 30Nm that can exceed 100Nm for short periods. With a reduction ratio of 10.9 and torque exceeding 1100Nm, the central mechanism is capable to warp the robot of 45° in only one second, which is fifteen times faster than the small-scale version V1. This problem can be avoided by adjusting acceleration ramps in the Curtis 1228 DC controllers, that modulate intensities up to 70A. Two or four 12V 48Ah on-board batteries store the energy. V3 is also equipped with a central electric clutch that allows to decouple the warping mechanism when rolling and to guarantee contact for the four wheels on irregular ground (no overconstraint).

3.7 Control and Sequential geometric model

OpenWHEEL i3R can be tele-operated on smooth terrain. However, the step-climbing process is complex and is supposed to be left completely automatic. The pilot has only to choose when to trigger climbing. An approximate control in open loop of the robot was made for OpenWHEEL V1 based on the sequence presented in Fig. 11. Open WHEEL V2 and 3 are controlled in closed loop and use a more detailed sequential geometric model. This requires to write a 3D geometric model for each of the 19 stages. This allows to adjust the model according to the scale of the considered robot and to tune the control strategy to the dimensions of the obstacle. Doing so, smaller obstacles will be crossed with smaller motions, which means a faster, more energy efficient and more stable climbing process.

Table 5: List of geometric parameters for the different versions of robots.

Name	**Definition**	**OW V1**	**OW V2**	**OW V3**
b	Wheelbase length T_1T_2	175 mm	260 mm	1210 mm
t	Track width $O_{a1}O_{a2}$	190 mm	151 mm	1250 mm
r_w	Wheel radius	25 mm	25 mm	190 mm
h_l	Leg height	72 mm	105 mm	500 mm
m	Mass	1530 g	2330 g	< 200kg
k_0	Reduction ratio for central joint	560	35	10,9
k_w	Reduction ratio for the wheels	15	3	1,3

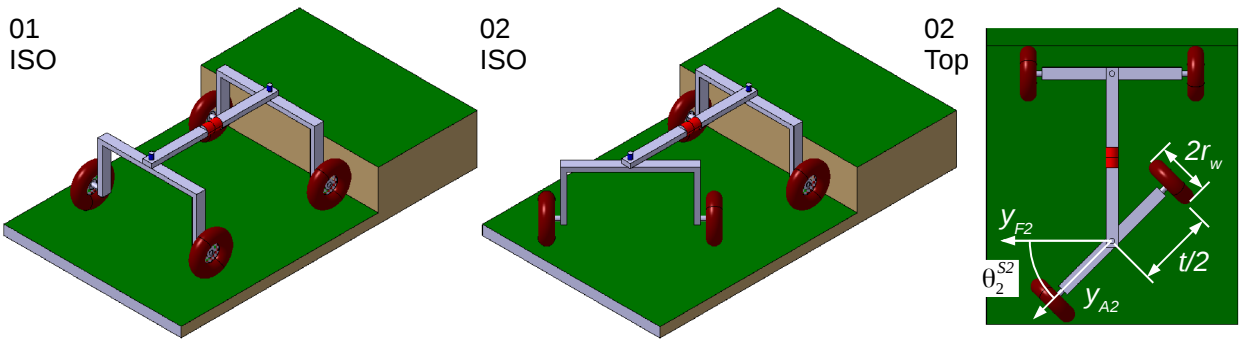

Figure 16: Model for steering reconfiguration at stage 2.

Design parameters: The considered design parameters characterizing geometry and scale of the different versions are summarised in Table 5.

Steering reconfiguration for stability: Before lifting the exploring wheel, the stability margin must be increased by steering the other axle. This is done at stages 2, 6, 11 and 15, that is to say the first stage of the climbing phase of each wheel. For instance for stage 2 (Fig. 16), the required steering angle of axle 2 is denoted θ_2^{S2} and must be smaller than $\theta_{a\,max}$, which is defined at $\pi/4$ for design reasons and to avoid the singular configuration where all contact points P_{as} are aligned. The kinematics equation (7) based on rolling without slipping of wheels (W_{a2}) gives the opposite rotations θ_{21}^{S2} and θ_{22}^{S2} of the wheels required to generate the steering angle θ_2^{S2} for stage 2. It is also written in actuator configuration space.

$$\theta_{21}^{S2} = -\theta_{22}^{S2} = t\,\theta_2^{S2}/2\,r_w \quad \Leftrightarrow \quad \theta_{act\,21}^{S2} = -\theta_{act\,22}^{S2} = k_w\,t\,\theta_2^{S2}/2\,r_w \tag{7}$$

However, it is not safe to rely on the non-slipping hypothesis. Using the additional steering rotation sensor, a much more robust solution is to increase θ_{21}^{S2} and decrease θ_{22}^{S2} at the same rate until the steering angle θ_2^{S2} reaches the expected value $\theta_{a\,max}$.

Steering-warping coupling: Steering-warping coupling is a phenomenon that concerns stages 6, 11 and 15. In order to anticipate the lifting of the exploring wheel (W_{as}), the other axle $(A_{a'})$ has to be steered. When the robot is not horizontal any more (*i.e.* the steering axis $z_{Aa'}$ is no more normal to the ground plane), the wheels of axle $(A_{a'})$ cannot stay in the plane of the ground after steering, and one contact is lost. This can be solved by a corrective warping of R_0.

For example at phase 6 (Fig. 17), if the front frame (F_1) is supposed fixed to the ground and submitted to a roll angle α and a pitch angle β with respect to the fixed frame $(T_{1,}x_{0,}y_{0,}z_0)$, the wheel-centre point O_{21} is calculated by the product

$$O_{21} = R_y(\beta).R_x(\alpha).T_x(-b/2).R_x(\theta_0).T_x(-b/2).R_z(\theta_2).T_z(-h_l).T_y(-t/2).T_1 \tag{8}$$

with R and T being homogeneous matrices for rotation / translation and T_1 being the point defined in Fig. 10. The vertical coordinate of O_{21} in the ground frame $(T_{1,}x_{0,}y_{0,}z_0)$ is given by (9).

$$z_{O21} = \cos(\beta)[\cos(\alpha)(\frac{-t}{2}\sin(\theta_0)\cos(\theta_2) - h_l\cos(\theta_0)) + \sin(\alpha)(\frac{-t}{2}\cos(\theta_0)\cos(\theta_2) - h_l\sin(\theta_0))] - \sin(\beta)[\frac{t}{2}\sin(\theta_2) - b] \tag{9}$$

z_{O22} can be deduced from (9) by replacing parameter t by $-t$. The difference of altitude between O_{21} and O_{22} does not depend on b and h_l and can be simplified into (10).

$$z_{O22} - z_{O21} = t[\cos(\beta)\cos(\theta_2)\sin(\alpha+\theta_0) + \sin(\beta)\sin(\theta_2)] \tag{10}$$

As the track width *t* is positive, the condition to keep O_{21} and O_{22} at the same altitude is given by (11).

$$\boxed{\sin(\alpha+\theta_0) = -\tan(\beta)\tan(\theta_2)} \tag{11}$$

As angles α and β can be measured with a 3D accelerometer fixed to the front frame (F_2) and used as an inclinometer, equation (11) allows to extract the corrective warping θ_0 for a given steering θ_2.

Lifting the exploring wheel: An exploring wheel is lifted at stages 3, 7, 12 and 16, which represent the 2nd stage of each climbing phase. Lifting is controlled by θ_0 and calculated in (12) for stage 3 (Fig. 18a).

$$\theta_0^{S3} \approx asin(h_s/t) \tag{12}$$

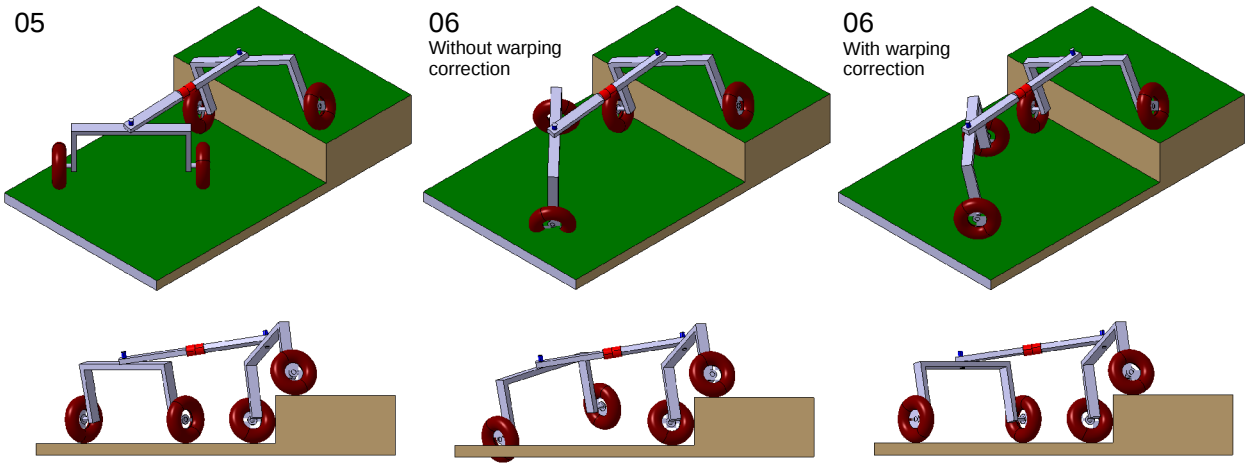

Figure 17: Model for steering-warping coupling.

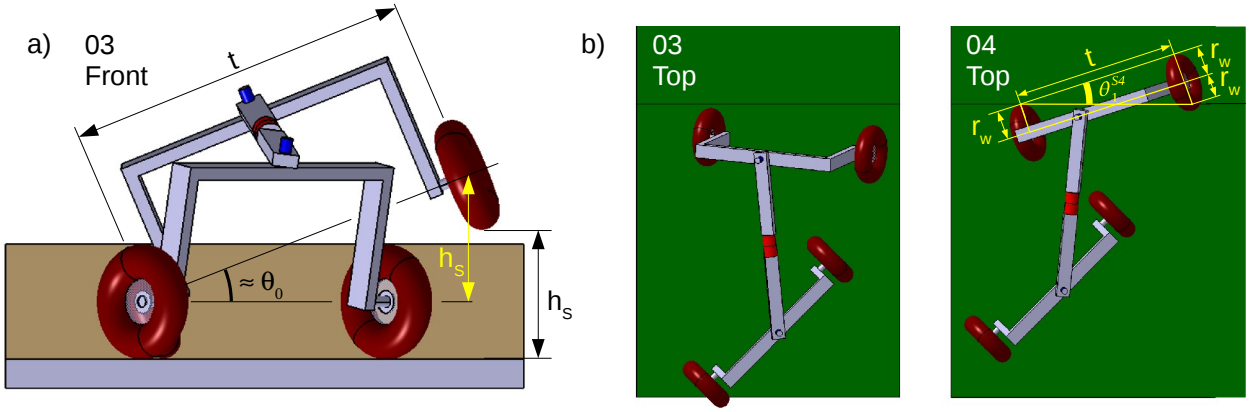

Figure 18: Model for: (a) lifting the exploring wheel; (b) pushing the wheel over the obstacle.

Pushing the exploring wheel over the obstacle: An exploring wheel is pushed over the obstacle at stages 4, 8, 13 and 17, which are the third stage of each climbing phase. For stage 4 (Fig. 18b), the exploring wheel (W_{11}) is pushed forward by axle (A_2) until it lays completely over the step in top view, which leads to a limit on the front steering angle θ_1 given by equation (10).

$$\theta_1^{S4} \approx atan(2r_w/t) \tag{13}$$

Landing the exploring wheel on the obstacle: An exploring wheel lands on top of the obstacle at stages 5, 9, 14 and 18, that are the fourth and last stage of the climbing phase of each wheel. Landing is controlled by θ_0 in a similar way as lifting with equation (12).

3.8 Conclusion on agile obstacle crossing at low speed

This section presented the OpenWHEEL i3R mobile robot, a rover capable to roll on regular ground and to climb step-obstacles as high as two-thirds of its centre of gravity. OpenWHEEL i3R is interesting as it combines the rolling efficiency of the wheeled propulsion to the agility of the legged locomotion, with a simple control based on minimal actuation of the four wheels and only one central warping actuator. Three demonstrators were built to demonstrate the concept: two at small scale and one at full scale, comparable to a commercial vehicle such as an ATV. A sequential geometric model was built, based on a 3D geometric model for each stage. Control is based on the position of the joints and the main required equations are given here for lifting, pushing and landing the exploring wheel over the obstacle. Parasite phenomena and their associated equations are also identified, such as the negative effect of pitch angle, cured by a proper mass repartition, and steering-warping coupling, cured by an adjustment in warping

control. The tests on the demonstrators are very encouraging and open perspectives on designing new highly efficient wheeled robots and vehicles for agile mobility on all-terrain and clearance performance.

4. High speed safe control based on dynamic stability

Sections 2 and 3 focused mostly on low speed motion (a few km/h), and it was shown that all-terrain capabilities can be improved by a suitable mechanical analysis and design. However, motion in all-terrain can also be fast. This section shows a different approach based on control to improve vehicle dynamic stability.

4.1 Vehicle Lateral dynamic stability

The growing popularity of light All-Terrain Vehicles (ATVs) over the last decade, together with their propensity to rollover, invites to consider the design of on-board safety devices in order to reduce especially lateral rollover fatalities. In the same time, off-road mobile robots appear as an interesting solution so as to answer social needs in various fields of application such as farming and surveillance [Siegwart 04]. Benefit on work accuracy and improved safety can be expected from innovation in mobile robotics. However, such applications require highly accurate control laws, able to preserve vehicle stability even at high speed.

Indeed, in ATVs and off-road mobile robot context, the complexity and the variability of the encountered phenomena have to be tackled to ensure both accuracy and security. Nevertheless, if numerous systems have been developed for road vehicles (active suspensions, active steering [Bosch 06], steering and braking control [Ackermann 98] and [Schofield 06]), they appear to be poorly relevant for fast off-road motion context since they do not adapt to varying grip conditions. Consequently, specific safety devices have to be designed.

The first step in the development of such devices is the design of a rollover indicator including grip condition variations. Previous work [Bouton 07-3] has shown that the Lateral Load Transfer (LLT – [Gaspar 05]) is a very relevant criterion. Its advantages, with respect to other stability metrics such as the Static Stability Factor (SSF) [NHTSA 05], the force-angle measurement criterion [Papadopoulos 96, Diaz-Calderon 06] or the Zero Moment Point (ZMP - proposed usually to investigate humanoid and mobile robots stability, [Sardain 04]) are that, on the one hand it does not demand for a huge and expensive perception system (which would be incompatible with ATV applications), and on the other hand it is not dependent on some thresholds particularly difficult to tune in outdoor environment. A backstepping observer, taking into account sliding effects, has then been proposed in [Bouton 08] in order to estimate on-line the LLT criterion, as well as its expected values on some horizon of prediction, so that imminent rollover situations can actually be detected.

In this section, this indicator is used as a basis for designing an active anti-rollover device dedicated to ATV and off-road mobile robots. More precisely, the maximum vehicle velocity ensuring that the LLT remains within a safety range over the horizon of prediction is estimated on-line, and can then be applied to the vehicle actuator in order to avoid imminent rollover. The algorithm relies on Predictive Functional Control principle (PFC – [Richalet 93], [Vivas 05]).

The section is organized as follows: vehicle modeling in presence of sliding is first recalled. Next, Predictive Functional Control principle is applied to control vehicle velocity in order to guarantee lateral dynamic stability on slippery ground of both ATV and mobile robots. Finally, real experimentations on a fast off-road mobile robot are reported and show the relevancy of the proposed approach in situations where lateral rollover is imminent.

4.2 Dynamic model of the vehicle

In order to describe the rollover of a mobile robot or ATV, its motion in yaw and roll frames has to be known. As a result, two representations are here introduced: one is a yaw representation (Fig. 19) and the other one is a roll representation (Fig. 20). The yaw model aims at describing the global vehicle motion on the ground and consists of an extended bicycle model. This first part of the model is used to estimate some vehicle motion variables (such as the lateral acceleration of the vehicle center of gravity) and

sideslip angles (according to a backstepping observer described in §4.5). These variables are then injected into the second part of the dynamic model, characterized by a roll 2D projection (shown on Fig.2), used to compute roll angle, roll rate and the *LLT*.

The notations used in this paper, and reported on Fig. 19 and Fig. 20, are listed below:

- $R_0(x_0,y_0,z_0)$ is the frame attached to the ground, $R_1(x_1,y_1,z_1)$ is the yaw frame attached to the vehicle, $R_2(x_2,y_2,z_2)$ is the roll frame attached to the suspended mass,
- ψ is the vehicle yaw angle, φ_v is the roll angle of the suspended mass and δ is the steering angle,

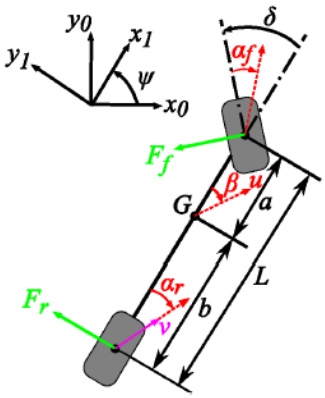

Figure 19: Yaw projection.

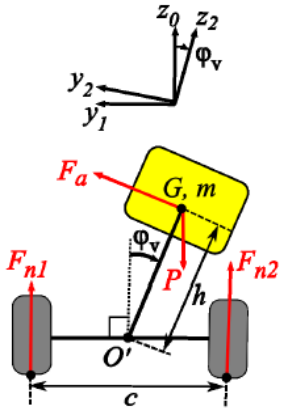

Figure 20: Roll projection.

- $\beta, \alpha_r, \alpha_f$ are the global, rear and front sideslip angles,
- v is the linear velocity at the center of the rear axle and u is the linear velocity at the center of gravity,
- a and b are the front and rear vehicle half-wheelbases (L=a+b is the vehicle wheelbase), c is the vehicle track and h is the distance between the roll center O' and the vehicle center of gravity G,
- I_x, I_y, I_z are the roll, pitch and yaw moments of inertia of the suspended mass assumed to be symmetrical with respect to the two planes (z_2, y_2) and (x_2, y_2).
- P=mg is the gravity force on the suspended mass m, with g denoting the gravity acceleration,
- F_f and F_r are the front and rear lateral forces,
- F_{n1} and F_{n2} are the normal component of the tire/ground contact forces on the vehicle left and right sides,
- F_a is a restoring-force parametrized by k_r and b_r, the roll stiffness and damping coefficients:

$$\overrightarrow{F_a} = \frac{1}{h}\left(k_r\varphi_v + b_r\dot{\varphi}_v\right)\overrightarrow{y_2} \tag{14}$$

The roll stiffness k_r and the distance h are assumed to be preliminary calibrated. The roll damping b_r is experimentally evaluated (through a driving procedure) and the other parameters (wheelbase, weight, etc) are directly measured.

4.3 Motion equations

Motion equations issued from the yaw projection shown on Fig. 19 require analytical expressions of lateral forces F_f and F_r. Therefore, as explained in [Bouton 08], a simple linear tire model has been considered. It can be expressed as:

$$\begin{cases} F_f &= C_f(.)\alpha_f \\ F_r &= C_r(.)\alpha_r \end{cases} \tag{15}$$

This model requires only the knowledge of the front and rear cornering stiffnesses ($C_f(.)$ and $C_r(.)$) essentially dependent on grip conditions and normal tire/ground contact forces. In order to reflect both the

non linear behavior of the tire and grip condition variations, $C_f(.)$ and $C_r(.)$ are considered as slowly varying (compared to sideslip angles) and on-line estimated thanks to the observer briefly described in §4.5. Only one parameter is then needed, contrary to classical tire models such as the celebrated Magic formula [Pacejka 06]. The dynamic equations of the yaw model [Stéphant 04] can be expressed as:

$$\begin{cases} \ddot{\psi} &= \frac{1}{I_z}\left(-aC_f\alpha_f\cos(\delta) + bC_r\alpha_r\right) \\ \dot{\beta} &= -\frac{1}{um}\left(C_f\alpha_f\cos(\beta-\delta) + C_r\alpha_r\cos(\beta)\right) - \dot{\psi} \\ \alpha_r &= \arctan\left(\tan(\beta) - \frac{b\dot{\psi}}{u\cos(\beta)}\right) \\ \alpha_f &= \arctan\left(\tan(\beta) + \frac{a\dot{\psi}}{u\cos(\beta)}\right) - \delta \\ u &= \frac{v\cos(\alpha_r)}{\cos(\beta)} \end{cases} \tag{16}$$

4.4 Lateral Load Transfer computation

The general expression of the Lateral Load Transfer LLT [Miège 02] is:

$$LLT = \frac{F_{n1}-F_{n2}}{F_{n1}+F_{n2}} \tag{17}$$

Clearly, a rollover situation is detected when a unitary value of LLT is reached, since it corresponds to the lift-off of the wheels on the same side of the vehicle. Here, the vehicle behavior will be considered as hazardous when LLT reaches the critical threshold 0.8. In order to extract normal force expressions from the roll model (Fig. 21), the following assumptions have been made:

- The entire vehicle mass is suspended, which implies insignificant non-suspended mass,
- Sideslip angles α_r, α_f and β are assumed to be small (corroborated by experiments). As a consequence, the vehicle velocity u at roll center can be considered to be equal to the rear axle one (i.e. $u \approx v$), see (16).

Using these assumptions, the LLT indicator can be evaluated from the Fundamental Principle of the Dynamic (FPD) applied to the overall system. More precisely, variations of φ_v, F_{n1} and F_{n2} can be derived as:

$$F_{n1} + F_{n2} = m\left[-h\ddot{\varphi_v}sin(\varphi_v) - h\dot{\varphi_v}^2cos(\varphi_v) + g - \left(\frac{k_r\varphi_v + b_r\dot{\varphi_v}}{mh}\right)sin(\varphi_v)\right]$$

$$F_{n1} - F_{n2} = \frac{2}{c}\left[I_x\ddot{\varphi_v} + (I_z - I_y)\left[\dot{\psi}^2cos(\varphi_v)sin(\varphi_v)\right]hsin(\varphi_v)(F_{n1}+F_{n2})\right] \tag{18}$$

$$\ddot{\varphi_v} = \frac{1}{hcos(\varphi_v)}[h\dot{\varphi_v}^2 \sin(\varphi_v) + h\dot{\psi}^2sin(\varphi_v) + u\dot{\psi}cos(\beta) + \dot{u}sin(\beta) + u\dot{\beta}cos(\beta) - \left(\frac{k_r\varphi_v + b_r\dot{\varphi_v}}{mh}\right)cos(\varphi_v)]$$

In order to infer the roll angle and the LLT from (18), the global sideslip angle and the yaw rate are both required. Since the former one cannot be measured, a backstepping observer has been designed.

4.5 Grip conditions estimation

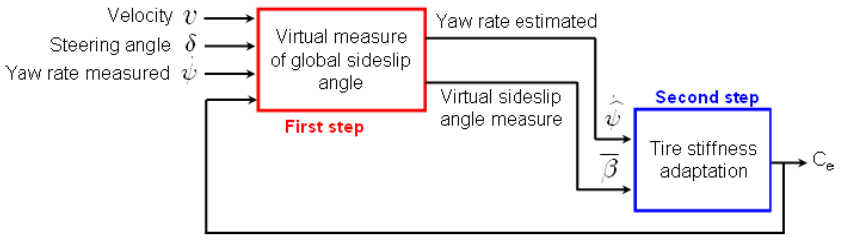

Figure 21: Backstepping approach principle.

In order to account for both tire/ground contact non-linearities and grip condition variability, a backstepping observer has been proposed in previous work [Bouton 08]. It can be summarized by the scheme depicted on Fig. 21. The observer permits to estimate the global sideslip angle ($\bar{\beta}$), the yaw rate ($\hat{\dot{\psi}}$) and a global tire cornering stiffness (C_e) based on three available measurements: the yaw rate $\dot{\psi}$ (available from a gyrometer), the rear axle linear velocity v(from a Doppler radar) and the steering angle δ (from a steering angle sensor).

4.6 Predictive Functional Control of vehicle velocity - Strategy of LLT limitation

In order to avoid the rollover risk, the limitation of the LLT (i.e. $LLT \leq 0.8$) through the control of the vehicle speed is here investigated. The idea is to compute at each time the velocity leading to this LLT threshold one moment in the future. This value can then be considered as the maximum admissible velocity (denoted v_{max} in the sequel) to avoid lateral rollover situation (Fig. 22).

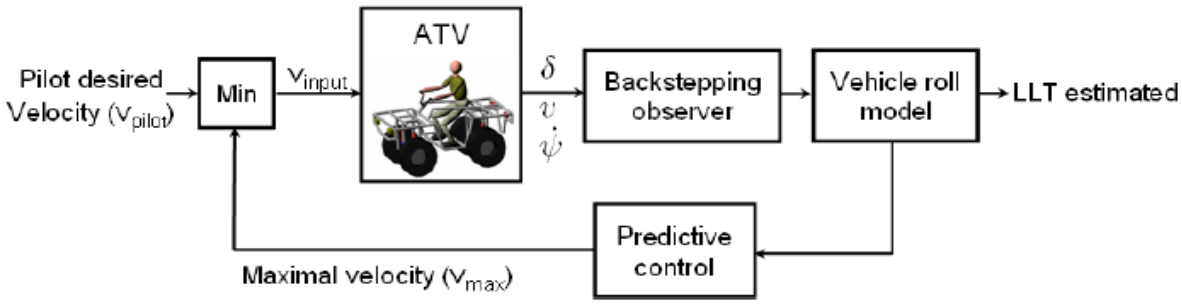

Figure 22: Velocity control of an ATV or mobile robot.

The computation of the maximum velocity, detailed hereafter, is represented by the block ``Predictive control". Relying on this variable, the speed limitation process consists on the following steps:

- The ``Min" block supplies the rear axle linear velocity control input v_{input} to be applied to the vehicle. This variable is deduced from the comparison between the velocity specified by the pilot (ATV) or desired (autonomous mobile robot) $v_{desired}$ and the maximum velocity v_{max}: $v_{input} = \min(v_{desired}, v_{max})$
- The three measurements shown on Fig. 22 are then used to estimate on-line the sliding parameters and the global cornering stiffness thanks to the backstepping observer,
- Then, the global cornering stiffness, the measured rear axle linear velocity and the measured steering angle are reported into the vehicle roll model in order to compute the roll angle φ_v and the LLT (see (18)),
- Finally, the roll angle φ_v, the sliding parameters and the steering angle are processed in the ``Predictive Control" block in order to supply the maximum velocity.

In order to anticipate and then avoid hazardous situations, the computation of v_{max} is based on the Predictive Functional Control (PFC) formalism, detailed in [Vivas 05]. The vehicle velocity is then viewed as a control variable and v_{max} is designed to ensure the convergence of the LLT towards 0.8.

4.7 Predictive maximum velocity computation

As it can be seen in equations (18), the LLT does not rely explicitly on vehicle velocity, but on roll angle: vehicle velocity should then be designed to control φ_v.

The roll angle equation (18) is non-linear when PFC formalism requires linear equations [Richalet 97]. Therefore, as a first step it is necessary to approximate equation (18) to a linear model. In the sequel, φ_{NvL} and φ_{vL} denote the roll angle supplied respectively by non-linear model (18) and by the linear model to be derived. As in [Bouton 09], linearization of (18) leads to:

$$\ddot{\varphi_{vL}} = \frac{1}{h}\left[u^2\cos(\beta)\left(\frac{\delta+\alpha_f-\alpha_r}{L}\right) - \left(\frac{k_r\varphi_{vL}+b_r\dot{\varphi_{vL}}}{mh}\right)\right] \quad (19)$$

PFC algorithm is now applied to linear system (19) in order to derive the maximum velocity. The principle of the predictive approach is summarized in [Bouton 09]. Roughly, it consists in finding the control sequence which permits to reach "at best" the future set point after a specified horizon of prediction H. More precisely, the algorithm consists in the following steps:

1. The first step consists in computing the roll angle value, hereafter denoted $\varphi_{vtarget}$ leading to a LLT steady state value equal to the critical threshold 0.8. As in [Bouton 09], $\varphi_{vtarget}$ is approximated by:

$$\varphi_{vtarget} = \pm arcsin\left(\frac{0.8c}{2h}\right) \quad (20)$$

2. Next, a desired reference trajectory φ_{vRef}, joining the current state φ_{vNL} to $\varphi_{vtarget}$ during the horizon of prediction is defined. Typically a first order discrete system is considered:

$$\varphi_{vRef_{[n+i]}} = \varphi_{vtarget} - \gamma^i.\left(\varphi_{vtarget} - \varphi_{vNL_{[n]}}\right) \quad (21)$$

The subscripts $[n]$ and $[n+i]$ (with $0 \leq i \leq h$) denote respectively the current time instant t and successive future time instants up to $t+H$ (since $[n+H]$ corresponds to time instant $t+H$) and γ is a parameter tuning the settling time for the reference trajectory to reach the set point.

3. Then, at each sample time, an optimal control sequence ($w_{[n]},...,w_{[n+h]}$) bringing φ_{vL} to $\varphi_{vtarget}$ is computed through the minimization of a quadratic criterion hereafter noted $D_{[n]}$. Moreover, since the linearization of equation (18) introduces some approximations that necessarily impair the accuracy of the predicted values of the roll angle and then of the LLT, the extended criterion $D_{[n]}$ incorporates the current and expected discrepancies between the roll angle values supplied by the nonlinear model and the linear model:

$$D_{[n]} = \sum_{i=1}^{h}\left\{\widehat{\varphi_{vL}}_{[n+i]} + \widehat{e}_{[n+i]} - \varphi_{vRef}{}_{[n+i]}\right\}^2 \quad (22)$$

where $\widehat{\varphi_{vL}}_{[n+i]}$ denotes the predicted output process obtained from linear model and the control sequence and, where the future output error $\widehat{e}_{[n+i]}$ is defined as:

$$\widehat{e}_{[n+i]} = e_{[n]} = \varphi_{vNL_{[n]}} - \varphi_{vL_{[n]}}, \quad 1 \leq i \leq h \quad (23)$$

If the optimal control sequence obtained from the minimization of $D_{[n]}$ was applied over the horizon of prediction, then φ_{vL} and LLT would reach respectively $\varphi_{vtarget}$ and LLT_{limit} at time $t+H$. Therefore, the first element of the control sequence, i.e. $w_{[n]}$, has to be considered as the maximum control input value, and then the maximum vehicle velocity at sample time $[n]$ is $v_{max}=(w_{[n]})^{1/2}$.

4.8 Results

Since advanced simulation results, obtained with the predictive functional control law and a virtual quad bike, have already been presented in [Bouton 09], this subsection presents real experiments performed with the robot described in Fig. 23. It consists of an electric off-road vehicle, whose weight and maximum speed are respectively 350kg and currently 8m/s. The main on board exteroceptive sensors are a gyrometer fixed on the chassis and supplying a yaw rate measurement accurate to within 0.1°, a steering angle sensor and a Doppler radar.

Then, with the experimental platform described above, a reference trajectory was manually recorded (the reference trajectory can be followed by using path tracking algorithm developed in [Lenain 07]): it is composed of a straight line connected smoothly to a curve with a constant 4.5m radius of curvature, see Fig. 24. More precisely, two tests have been performed: the first one consists in using path tracking control without predictive control and a constant v_d=6 $m.s^{-1}$ velocity. The second test consists

in using the predictive functional control algorithm dedicated to LLT limitation with v_d=6 $m.s^{-1}$, H=1s (chosen according to the vehicle dynamic features), with 10 coincidence points (i.e. h=10), γ=0.2 and LLT_{limit}=0.35.

Figure 23: Experimental platform.

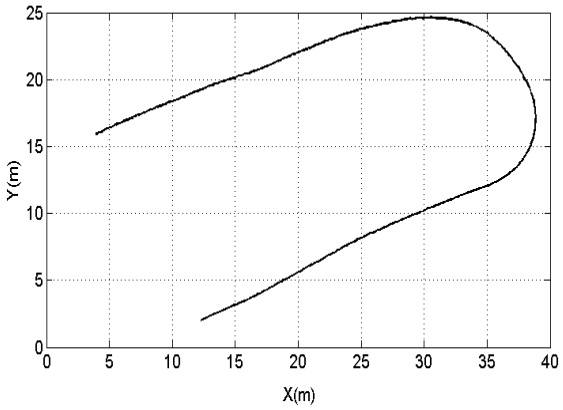

Figure 24: Reference trajectory.

Fig. 25 shows the time evolution of the measured velocity v_{m1} when path tracking is done without velocity control (v_{m1}≈ v_d≈ 6$m.s^{-1}$ after settling time) in black dash-dotted line, the maximum velocity v_{max} (computed with the PFC algorithm, in red solid line) and the rear axle velocity v_{m2} measured on the vehicle (in green dashed line) when velocity control is used. As described in Fig. 25, v_{m2} is supposed to be equal to the minimum of v_d and v_{max}. From t=0s to t=5.8s, v_{m2} is equal to v_d. Then, between t=5.8s to t=9.2s, during the curved part of the reference path, the velocity control variable applied to the vehicle is the maximum velocity given by the predictive functional control algorithm. However, due to the delay introduced by the velocity actuator, the measured velocity v_{m2} is satisfactorily superposed with v_{max} only beyond t=7.8s. Finally, after t=9.8s, v_{max} is superior to the desired velocity, so that v_d can again be actually applied and after settling time t=13s, the measured velocity v_{m2} converges to v_d .

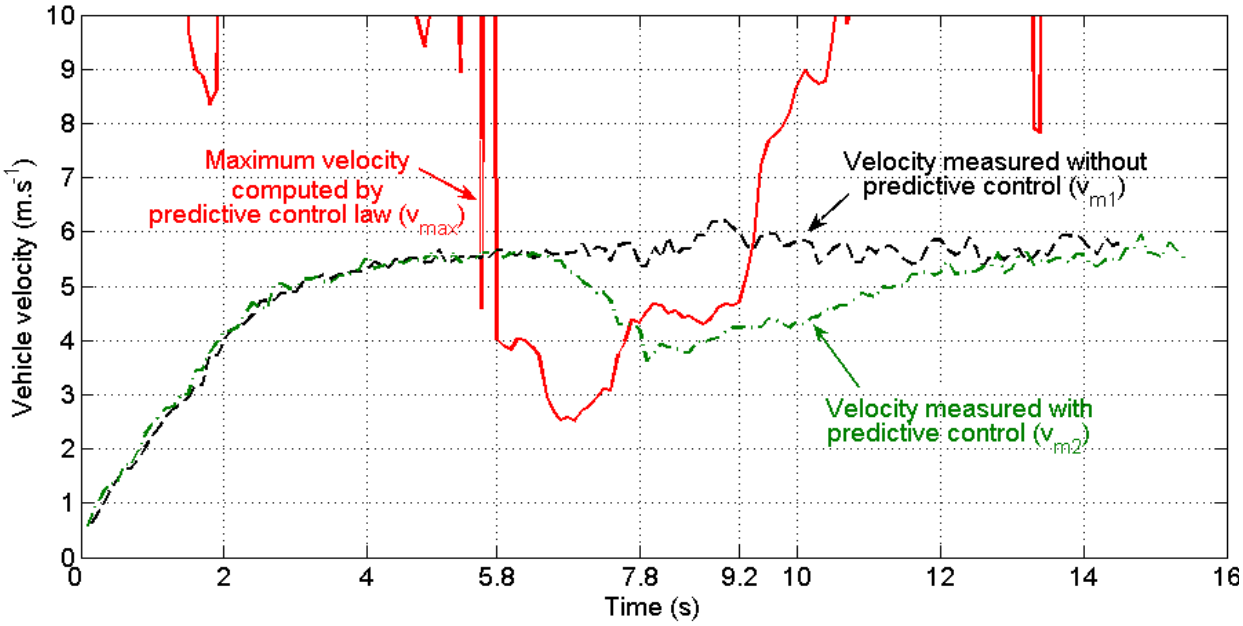

Figure 25: Velocity results with or without Predictive Functional Control.

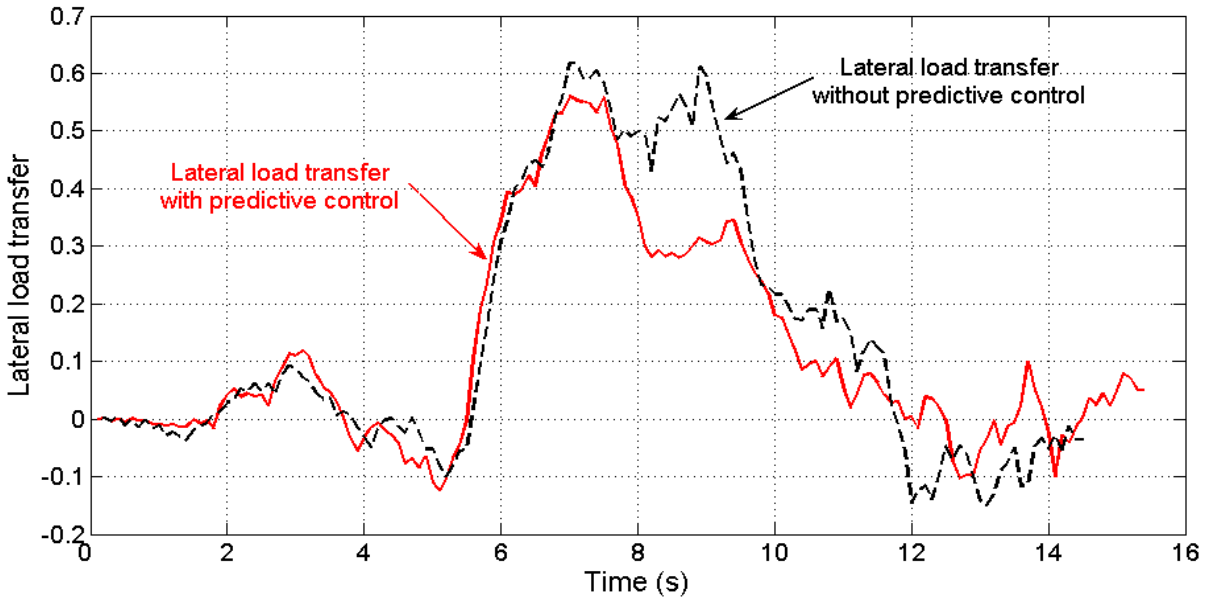

Figure 26: Lateral Load Transfer with and without Predictive Functional Control.

Fig. 26 shows the time evolution of the LLT without prediction (LLT obtained when $v_{m1} \approx v_d$ is measured on the vehicle and depicted in black dash-dotted line) and the LLT measured with the predictive control depicted in red solid line (LLT obtained with v_{m2}, *i.e.* when the minimum of v_d and v_{max} is applied to the vehicle). In this figure, the LLT obtained with v_{m1} is largely superior to LLT_{limit} fixed here at 0.35. On the contrary, after the settling time (after t=8s), the LLT measured with v_{m2} satisfactorily converges to the LLT_{limit}. Indeed, between t=6s and, t=8s the measured LLT is superior to the LLT_{limit}, since the velocity actuator introduces a delay between the velocity control variable, here equal to the maximum velocity v_{max} computed via PFC algorithm and the real velocity of the vehicle v_{m2}, as explained in the previous paragraph and which can be seen on Fig. 25. Finally, when the PFC is used, the measured LLT is equal to 0.35.

4.9 Conclusion on high speed safe control based on dynamic stability

This work proposes a new safety device, based on Predictive Functional Control formalism, dedicated to All-Terrain Vehicles and off-road mobile robots operating on a natural and slippery ground. First, previous work on path tracking control, built from both adaptive and predictive control laws, has been recalled. Sliding effects have been taken into account according to a backstepping observer adapting on-line the tire cornering stiffnesses of the front and rear tires. It enables to take into account the non-linear behavior of the tire and the variations in grip conditions when computing the sideslip angles. Then, these sliding parameters are introduced into a predictive functional control law, based on a vehicle dynamic model, so as to compute the maximum velocity admissible by the robot in order to ensure its lateral dynamic stability. Real experiments, carried out with a high speed mobile robot, demonstrate the applicability and the relevancy of the proposed control strategy to avoid rollover situations.

Future work will be dedicated to reduce the delay introduced by the velocity actuator. Indeed, it has been highlighted that the velocity measured on the vehicle differs from the velocity control variable. Therefore, another predictive control law based on the velocity actuator characteristics is under development so as to eliminate the delay.

Section 4 showed that the advanced control of an existing vehicle can lead to substantial improvements in behaviour, here for steering and rollover avoidance. Section 5 addresses another high-speed phenomenon: dynamic obstacle-crossing in all-terrain, more complex than slow obstacle-crossing (Section 3) that will require a suitable control as well as a deep mechanical re-design of suspensions.

5. INNOVATIVE SUSPENSIONS WITH 2 DOF FOR HIGH SPEED OBSTACLE CROSSING

Crisis conditions such as earthquake rescuing or de-mining operations require fast deployment and rapid analysis of broad areas of unstructured environment. In this context, a float of mobile, fast and inexpensive robots could be of great interest for extensive scanning of the area. One important problem to address is mobility on irregular grounds at fast speed. The FAST program of the French National Agency of Research is dedicated to the design and control of an innovative mobile robot, of about 1m and 150kg, capable to move at 10m/s on irregular grounds. Work is in progress on innovative mechanical architectures, as well as advanced control strategies. This section focuses on straight line motion and pitch angle stability during dynamic crossing of steep obstacles at 10 m/s.

Next subsection introduces the addressed types of grounds and obstacles. Afterward, a brief overview of the existing all-terrain suspensions is presented (§5.2). This shows relevance of the innovative concept introduced in §5.3: suspensions with two Degrees Of Freedom (DOF). Subections 5.4 and 5.5 present a 2D model of a complete vehicle rolling on an obstacle and the obtained results.

5.1 Addressed types of grounds and obstacles

The shape of ground can be modeled with several detail levels, depending on the size of the vehicle. Figure 27 presents two types of natural grounds. A structured ground (a) can be represented as a relatively smooth surface with certain order of continuity: 0 (C^0, no hole), 1 (C^1, tangential continuity) and possibly higher orders (C^2 for curvature continuity). On the contrary, an unstructured ground such as the one shown in (b) contains many bumps, holes and trees as well as cracks and cliffs of the landscape.

(a)  (b) 

Figure 27: Two types of natural grounds. (a) Structured ground. (b) Unstructured ground.

This introduces the notion of obstacle (Figure 28) as a local perturbation in the general shape of the ground. Positive obstacles (a,b,c) lay above the ground average surface whereas negative obstacles (d,e,f) lay beneath. Obstacles (a,d) that cannot be crossed by the considered vehicle are treated as walls (a) or holes (d) and represent a forbidden zone for the vehicle on the ground, that becomes locally non C^0. This work will focus on bumps (b,c), of height *h*. Case (b) will be treated in priority as it can be considered as a worst case of (c) because a wheel is designed to roll preferably on a C^1 surface.

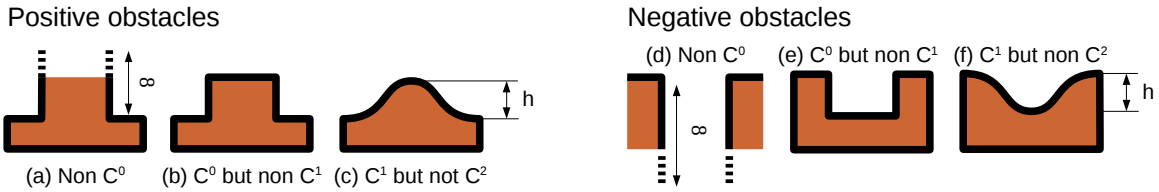

Figure 28: Six types of positive and negative obstacles.

Obstacle that respect conditions (24) and (25) are considered, with *r* the radius of the wheel.

$$h < r \quad (24)$$

$$h \sim r \quad (25)$$

Figure 29: Examples of existing all-terrain suspensions. (a) Ford F350 4x4 rigid axle suspension. (b) Mini-Baja vehicle at Oregon State University with double wishbone suspension.

(24) comes from the geometry of the wheel and means that a given obstacle of height *h* can be cross-able or not depending on the radius of the wheel of the vehicle. This means that even what is considered as a structured landscape by a man (Figure 27 (a)) may become unstructured for a vehicle of a lower scale. (25) is a rather ambitious objective as most of the wheeled vehicles have difficulties to dynamically cross obstacles as high as 30% of the wheel radius. Condition (25) means the maximal crossing-capacity of the wheel is researched, mostly by adding appropriate suspensions. It must also be noticed that an obstacle may be easy to cross at speed V_1 = 10m/s and impossible to cross without an accident at speed $V_2 > V_1$.

5.2 Existing all-terrain suspensions

Modern suspensions aim to improve dynamic behavior of vehicles in a wide range of driving conditions. Depending on the application, all-terrain mobile robots have additional requirements such as running-off-road, crossing obstacles, climbing and running at high speed. According to [Halconruy 95, Reimpell 01], suspensions can be classified in two categories:

- Rigid and semi-rigid axle suspensions (Figure 29a) were the first to appear and are still used on all-terrain vehicles. These suspensions are dedicated to commercial heavy vehicles. They can have a whole series of disadvantages that are unacceptable in passenger cars, but which can be admitted in commercial ones. However, they are more efficient to support high loads.
- Independent wheel suspensions (Figure 29b) such as double wishbone suspensions, McPherson strut suspension, rear axle trailing-arm suspension, semi-trailing-arm axles and multi-link suspensions are supposed to be more comfortable and adjustable.

Some suspensions integrate actuators and are therefore qualified of “active suspensions”. Two examples are the Bose suspension [Bose 10], a McPherson derivative that replaced springs by electromagnetic actuators adapted from loudspeakers (Figure 30a), and the Michelin ActiveWheel [Michelin 08], that uses an actuated rack and pinion located inside the rim of the wheel (Figure 30b). These two suspensions are interesting to compensate local irregularities on a plain road. As they are active suspension, they require a lot of energy for the suspension actuators as well as a knowledge of the road profile and irregularities. Robustness of the actuators is a critical point in all-terrain and the vertical run of the wheel, limited by the diameter of the wheel in the case of ActiveWheel, should be as long as possible.

To our knowledge, it appears that most of the existing suspensions are passive ones. Although they are not as efficient as active suspensions, they have the advantage to be inexpensive, energy efficient, reliable and not to require any knowledge of the environment.

In the literature, many patents exist that describe innovative passive suspension systems. In [Cheek 09], a novel suspension system is developed for independent wheel control. The main objective of this system is to provide an independent suspension apparatus for an off-road vehicle that is capable of moving each wheel away and towards a frame or body member of such vehicle. Other works are aimed to

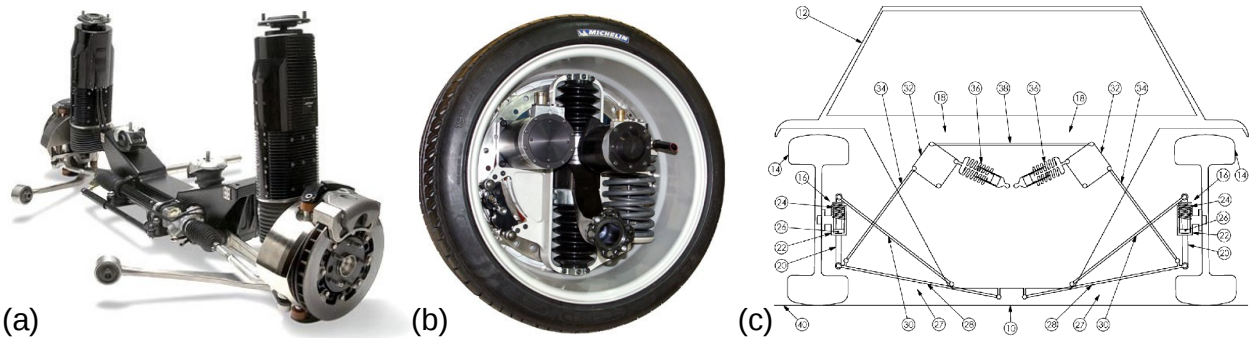

Figure 30: (a) Bose active suspension [Bose 10]. (b) ActiveWheel that integrates actuators for propulsion and suspension [Michelin 08]. (c) Two degrees of freedom suspension system [Sacli 09].

adjust vehicle suspension height to provide more ground clearance to the body work of the vehicle [McIntyre 09]. Other patented systems try to improve the performance of a shock absorber [Cox 09].

One original system is the suspension with two degrees of freedom presented in [Sacli 09]. This patent describes a new architecture which includes two sets of spring-dampers mounted along two different axes: vertical and slightly inclined lateral axes (Figure 30c). Such design combines a dive suspension with a roll suspension, including a locking linkage. This invention provides a suspension system that has good bump and dive camber control simultaneously with good roll camber control.

Many existing suspensions replace classical joints by rubber bushings, that allow small displacements in a horizontal plane for a better longitudinal comfort. However, displacements rarely exceed a few millimeters. From this overview, it is clear that the majority of suspensions, even active ones, do not improve longitudinal stability on rough terrain. Shocks against steep obstacles at high speed modify directly the horizontal vehicle dynamics, which is not addressed by most of the existing suspension systems, as they generally rely on shock absorbers mounted vertically with slight inclinations. For this reason, the main objective of this work is to present a mobile robot equipped with innovative suspensions dedicated to steep obstacle crossing at high speed and as passive as possible.

5.3 Innovative suspension

In [Fauroux 10-3], the analysis of a single wheel allowed to check the realism and the limits of the contact modeling in a multi-body dynamics software (Adams). It also showed that the horizontal forces cannot be neglected anymore with respect to the vertical ones in this type of obstacle crossing. Figure 31 shows the typical profile of the ground that should be addressed and the horizontal component of the normal vector gives an idea of the intensity of horizontal forces.

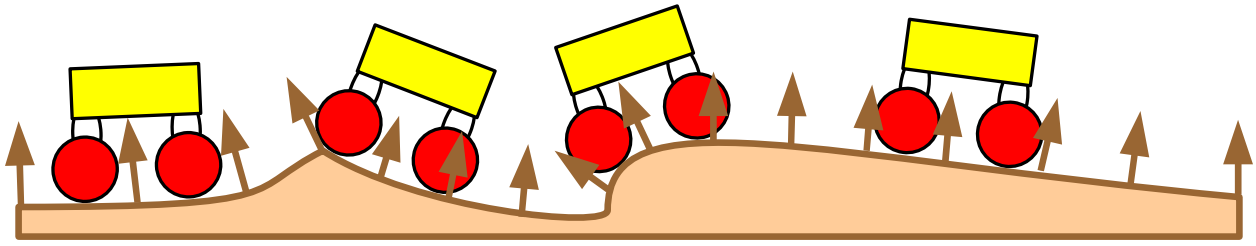

Figure 31: A typical case of ground profile for an all-terrain robot and the associated normal forces.

The natural consequence of this fact is that new suspensions will have to be designed in order tho absorb both vertical and horizontal contact forces. They could have many different implementations such as the one represented on Figure 32, using two cylinders in parallel, or even two prismatic joint serially connected, such as in the Adams model presented below in §5.4.

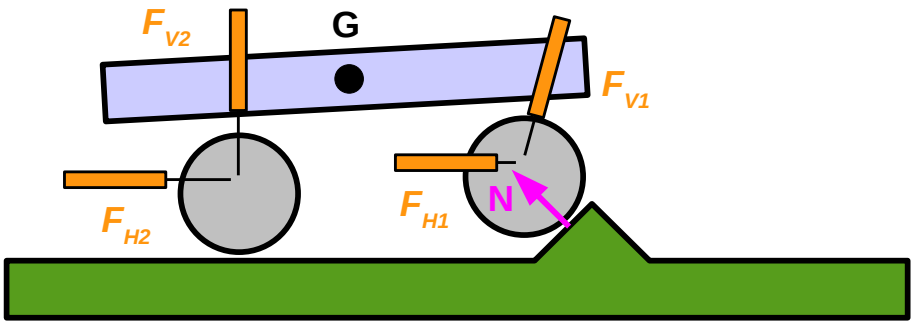

Figure 32: Concept of suspension with 2 Degrees Of Freedom (DOF) per wheel.

5.4 Two-wheel 2D model for pitch stability

The Adams model used to check the interest of 2 DOF suspensions is presented in Figure 33. Ground **0** is modeled by a 20m long plate, with an adjustable block on it for the obstacle. The chassis is made of two weighting spheres **1** and **2** that can be adjusted in mass independently. There were weighting 50 kg each for this work. The bar **3** guides the horizontal translation of cross-shaped sliders **4** and **5**. Two vertical rails **6** and **7** slide through parts **4** and **5** respectively. Wheels $\boldsymbol{W_1}$ and $\boldsymbol{W_2}$ are attached at the bottom of **6** and **7** by a revolute joint. Two needles **8** and **9** are soldered on the wheels as a guiding mark during rotation. All the parts from **3** to **9** have no mass. Although the model has a 3D view for better comprehension, it is a 2D model and is restricted to glide in the sagittal plane XZ.

The horizontal suspension $\boldsymbol{H_1}$ (respectively $\boldsymbol{H_2}$) connects part **3** and **4** (respectively **3** and **5**). The vertical suspension $\boldsymbol{V_1}$ (respectively $\boldsymbol{V_2}$) connects part **4** and **6** (respectively **5** and **7**). All the suspensions include both a spring and a damper. The vertical suspensions are pre-loaded of 500N each such that the chassis keeps its initial altitude. All the springs have vertical values of 5N/mm. Vertical damping was fixed to 3 Ns/mm while horizontal damping was reduced to 1Ns/mm in order to improve shock absorption. The values have an order of magnitude coming from ATV analysis and numerous simulations. The contact parameters have been tuned in a previous work [Fauroux 10-3]. Wheels weigh 5kg each and have radius $r_w = 250mm$. The running distance is $d_r = 10m$. The torque T allowing the vehicle to accelerate up to 10m/s after along distance d_r was found to be 110Nm for each axle. Lower values of T reach to higher values of d_r. They may also decrease the crossing capacity when the wheel crashes against the obstacle (a high normal force meaning a good lifting tangential force, even with small friction). Obstacle height is $h = 350mm$, a value that is interesting to push the suspension to its limits.

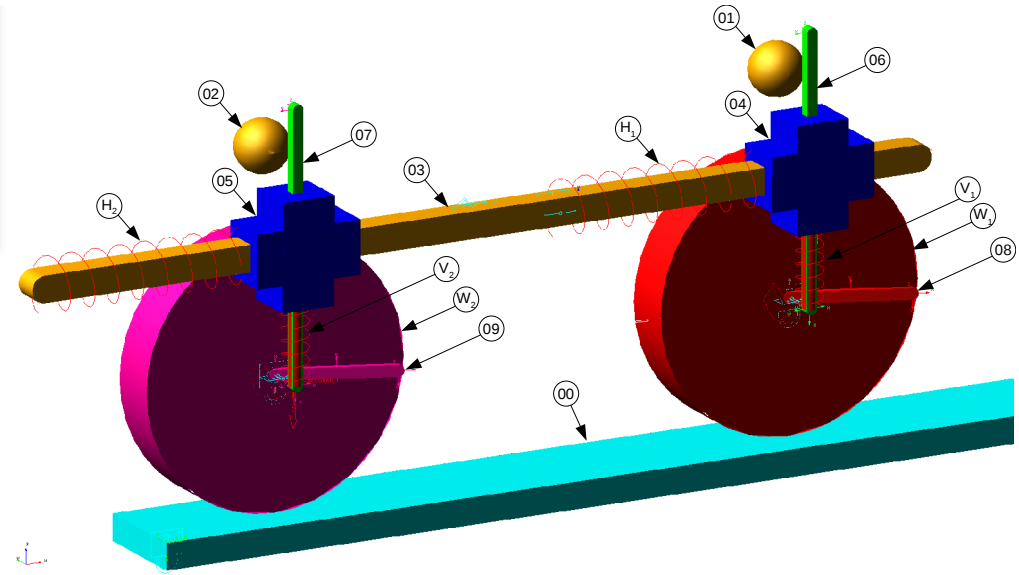

Figure 33: Adams model of a mobile robot with front and rear 2-DOF suspensions.

5.5 Simulation results

Some significant results are obtained by comparing three configurations of the mobile robot with suspensions including or not a horizontal mobility. The configurations are:

a) Without front horizontal suspension H1, without rear horizontal suspension H2;
b) With H1 but not H2;
c) With H1 and H2.

Motion capture of compared trajectories can be found in Figure 34.

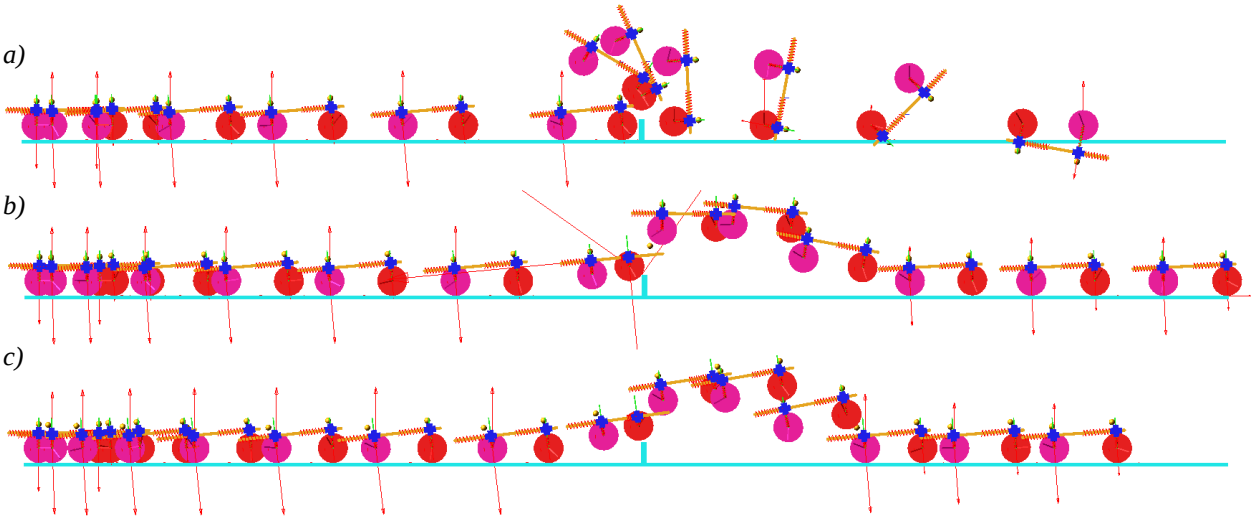

Figure 34: Motion comparison of three configurations with or without horizontal suspensions .

Only b) and c) configurations are stable. The shock with a vertical obstacle creates a horizontal reaction that is absorbed by H1, whereas it perturbs deeply the entire vehicle in case a) and causes tip-over. Figure 35 represents the compared pitch angles of the vehicles. It allows to differentiate case b), where the vehicle has a maximal pitch angle of -11.5° (nose landing), from case c), where the pitch angle reaches +11.2° (tail landing). Although configurations b) and c) are very close, nose landing is preferable because the driving torque applied to the wheels tends to nullify the pitch angle (auto-stability). In case of tail landing, the driving torque on the rear axle may cause instability. Torque transmission should be stopped or even reversed at landing. For all our models, the torque on rear axle was interrupted after 2s, at a time when the vehicle is in the air. This improved landing stability.

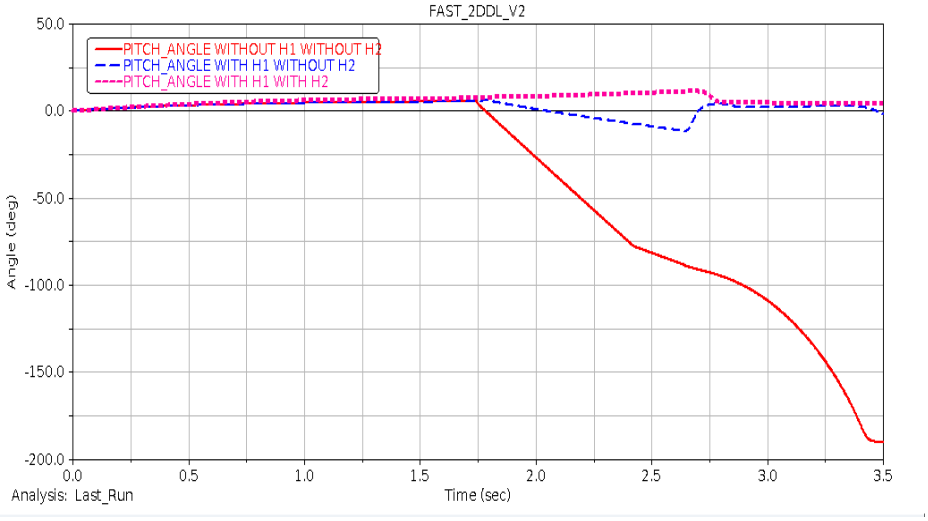

Figure 35: Comparison of pitch angle in three configurations with or without horizontal suspensions .

The horizontal suspension appears to be an important improvement for fast obstacle crossing. However, the front horizontal suspension H_1 has a bigger importance than the rear one H_2. The horizontal forces generally have two peaks corresponding to the first impact on the obstacle and then, to landing. The first peak on F_{H1} is generally higher than on F_{H2}. In case c), there was even no shock at all or the rear wheels against the obstacle (Figure 36). This is why suspension H_1 is vital to improve stability, whereas H_2 is optional. As the frontal shock may lead to lose two-thirds of the kinetic energy and half of the speed of the robot (Figure 36), H_1 must be reinforced relatively to H_2.

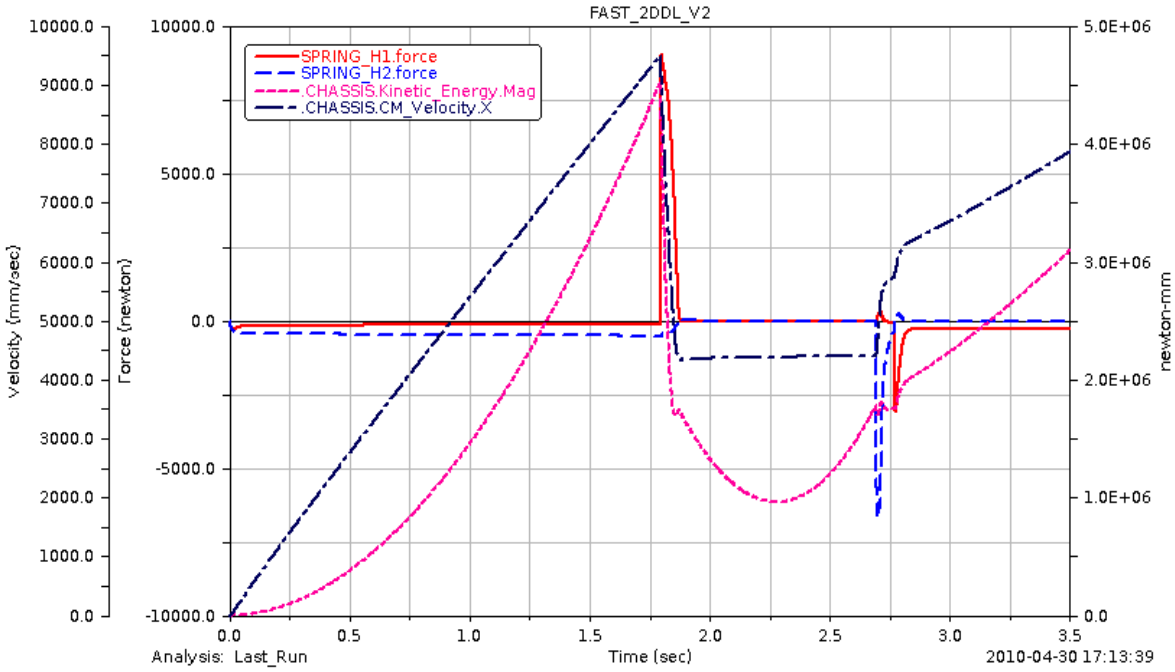

Figure 36: Force values of horizontal front (H1) & rear (H2) suspensions. Kinetic energy of the chassis.

5.6 Conclusion on high speed obstacle crossing

The originality of the proposed concept relies on a 2DOF suspension mechanism that adds a horizontal mobility to the classical vertical one. This supplemental mobility, combined with suitable stiffness and damping, allows to cross an obstacle higher than the radius of the wheel.

This result was obtained by simulation on a multibody software. A two-wheel 2D model was built and several configurations were tested. The ones with horizontal suspension showed very good crossing capacities, although the rear suspension seems to be less useful than the front one. This preliminary result will have to be checked on a prototype, as the shock phenomena are delicate to model accurately with multibody software. Future work will focus on defining the optimal stiffness and damping coefficients for a given obstacle and vehicle speed. Several options are possible, such as a passive suspension using fixed parameters, a semi-active suspension capable to adjust them with low energy consumption, or even an active suspension capable to inject peaks of force in the suspension when required. The first results are encouraging and a 0.5m long robot capable to reach 15m/s and named miniFAST is under construction. In a next step, automatic control scenarios will be implemented in order to keep the robot very stable during obstacle crossing, at speeds previously unachievable.

GENERAL CONCLUSION : TOWARDS NEW AGILE VEHICLES

This chapter presented four complementary research works on new strategies to build agile mobile robots in natural environment. Two principal functions were targeted: obstacle-crossing and steering.

Obstacles are one of the major difficulty of unstructured environments that can be found in natural or urban context. An obstacle is a local irregularity of the ground that cannot be crossed by

ordinary wheeled vehicles. Although obstacles depend on the considered locomotion speed and vehicle scale, the presented advances allow to improve the capacities of existing mobile robots and vehicles.

In section 3, it was demonstrated that a vehicle with wheels could cross very high obstacles at low speed. An original hybrid architecture was presented, consisting in four actuated wheels mounted on an articulated frame. Only one central actuator was used to make the four wheels successively cross the obstacle, which illustrates the concept of *minimal actuation* and guarantees both structure stiffness and easy control. A quasi-static climbing process divided into 19 stages was presented and experimented with our OpenWHEEL i3R robot, built in several versions and scales. It allowed to climb obstacles as high as 66% of the altitude of the centre of mass of the robot, independently of the diameter of the wheels. Future work will focus on longitudinal balancing, for even improved performance. The OpenWHEEL i3R robot demonstrates that a classical four-wheel architecture can be simply upgraded to an agile hybrid architecture, capable to bear heavy loads and keep them in equilibrium over high obstacles. This result is very encouraging and opens wide perspectives in agile vehicle design, with applications for transportation in natural and unstructured environment.

However, obstacle-crossing may become a challenge at higher speeds. Section 5 focused on the dynamic-crossing of obstacles at speeds close to 10 m/s. A new type of suspension mechanism was modeled, including a supplemental horizontal mobility allowing to cross steep obstacles. This mobility is used to dampen the horizontal component of the impact force, to increase the duration of the contact and to maintain a high normal force, thus avoiding slipping and using tangential force for obstacle ascension. A multibody model showed that a vehicle using this type of suspension was capable to cross obstacles as high as a wheel radius without any tip-over. This system should be installed on the front axle in priority, which is the first in contact with the obstacle. The authors are currently patenting a new suspension based on this concept but closely compatible with existing suspension architectures. It is expected that future vehicles could benefit from this concept for enhanced longitudinal stability and fast crossing capacities.

A rover in natural environment has to modify its trajectory by steering, another important function for autonomy. Although very simple and reliable on classical road vehicles, this function requires specific improvements in all-terrain to be performed efficiently and to be adapted to some particular steering principles.

In section 2 was considered the case of skid-steering, a steering principle compatible with all-terrain vehicles with many axles and robust swing-arm suspensions. A non-symmetric model of skid-steering was developed as well as an innovative suspension with dual configuration. It was implemented on a 6x6 all-terrain vehicle developed at IFMA. Experimental measurements of the contact forces confirmed the non-symmetry and showed that the energy consumption during steering could be decreased of 40% by a single adjustment of the kinematics of the suspensions, bringing a new repartition of normal and tangential frictional force over the axles of the vehicle. This encouraging result will allow to build a new vehicle capable to reconfigure its suspension during skid-steering for an improved efficiency. Doing this, the rover can be kept very simple and robust on rough terrain but also adjustable to the type of task and ground. More generally, rovers of the future will have to take into account the variability of the grounds and be capable to quickly adjust themselves for optimal operation.

Sections 2-3-5 were based on innovative mechanical design of new vehicles. Section 4 explored advanced strategies for the efficient control of existing all-terrain four-wheel vehicles, focusing on lateral stability and rollover avoidance during steering at high speed on natural and slippery ground. So as to develop a new active device, sliding effects have been taken into account according to a grip conditions observer. It enabled to take into account sliding effect when computing the sideslip angles. Then, sliding parameters were introduced into a predictive functional control law, based on a vehicle dynamic model, so as to compute the maximum velocity admissible by the robot, ensuring that the *Lateral Load Transfer* of the vehicle never exceeded the rollover threshold (i.e. $|LLT| \leq LLT_{limit}$). Real experiments, carried out with a high speed mobile robot, demonstrated the applicability and the relevancy of the proposed control strategy to avoid rollover situations.

In term of control, many complementary electronic devices appeared in the last decades, bringing new functions to road vehicles, such a anti-lock braking system or obstacle detection. However,

functional improvement may lead to a lack of reliability, that was observed for instance on speed regulators. This type of problem, although not critical on a road, may become a serious issue in all-terrain and lead to severe accidents. For this reason, the control of agile robots in all-terrain should be kept simple and robust. Section 4 showed that fast steering could be controlled with a good horizon of prediction from inexpensive sensors such as gyrometers. For low speed steering, the results from Section 2 can be achieved with even simpler control, as it requires only to put the suspension in a specific "turning configuration" during turns.

Obstacle crossing is generally a difficult task to control because it requires a preliminary knowledge of the obstacle. However, at least at low speed, the climbing strategy of the OpenWHEEL i3R architecture only requires to know the obstacle height, as all the stages depend on a pure geometric model (Section 3). The low number of actuators is also an advantage for simplicity. For obstacle-crossing at high speeds (10m/s), the reaction time should be around the millisecond, which requires a very fast control (Section 5). The simplest solution is to design a completely passive mechanism. For a higher degree of control, simple parameters such as suspension stiffness and damping coefficients may be adjusted at high speed, for optimal shock absorption as well as an an efficient wheel guidance on flat grounds. This traces improvements for future developments of this 2 DOF suspension and active suspensions in general.

From all these results, it can be seen that the wheeled locomotion has a bright future. Although very old and widely studied, wheeled locomotion remains one of the most energy-efficient locomotion modes on smooth terrain, but has a considerable extension potential in rough terrain. From complementary approaches based on kinematics, mechanical design, control and mechatronics, can be expected new generations of agile wheeled mobile robots with enhanced capacities. Natural environments provide very challenging conditions and agile vehicles allow a great number of useful applications for exploration, agriculture, transport and safety.

ACKNOWLEDGEMENTS

The Kokoon 6X6 prototype (Section 2) was designed, built, tested and continuously improved with the extensive help and constant motivation of IFMA and UBP students. The authors also acknowledge the financial support of OSEO-ANVAR (French National Agency for Development of Research), MICHELIN company and TIMS Research Federation. The other sponsors and people involved in Kokoon development are given on the Kokoon Project web page: http://www.kokoon.fr.st

For the OpenWHEEL i3R agile robot (Section 3), the authors wish to thank the TIMS Federation (Technologies for Innovation, Mobility and Safety) of Clermont-Ferrand University, France, for supporting the OpenWHEEL project. They also thank Region Auvergne & European Union for funding the OW project. Greetings to the following engineering students from 2006: G. Malval, E. Portales, M. Forlorou, S. Marco, Y. Koberle, D. Roux, L. Genevay, M. Tou, F. Bianchini, R. Cartailler, F. Hzag, S. Metais, C. Noellat. Thank you for your dedication & all-terrain help.

For Section 4 and 5, the authors wish to thank the French Research National Agency (ANR) for funding this work inside the FAST (FAST Autonomous Rover) project. They also thank the IFMA students that already contributed on the engineering aspects of Section 5: F. Kreit, A. Riesemann, A. Authier, S. Ovazza, R. Cousturier, T. Dejeante and R. Vendrome.

REFERENCES

Ackermann, J. and D. Odenthal. (1998). *Advantages of active steering for vehicle dynamics control*. In *International Conference on Advances in Vehicle Control and Safety*. Amiens: France.

Apostolopoulos, D.S. (2001). *Analytical configuration of wheeled robotic locomotion*. PhD Thesis, Carnegie Mellon University.

Bekker, M.G. (1969). *Introduction to terrain-vehicle systems*. The University of Michigan Press.

Besselink, B. C. (2003). Computer controlled steering system for vehicles having two independently driven wheels. *Computers and Electronics in Agriculture*, 39(3):209-226, August 2003.

Besselink, B. C. (2004). Development of a vehicle to study the tractive performance of integrated

steering-drive systems. *Journal of Terramechanics*, 41(4):187-198, October 2004.

Bosch, R. (2006). *Safety, comfort and convenience systems*. Hoboken, U.S.A.: Wiley. 404p.

Bose Systems. (2010). *Automotive active suspension*. Retrieved online April 2010, http://www.bosefrance.fr/FR/fr/learning-centre/suspension-problem

Bouton, N., Lenain, R., Fauroux, J.C., & Thuilot, B. (2007-1). *Dynamic modeling of all terrain vehicles designes for dynamic stability analysis.* In Proc. of Multibody Dynamics 2007, ECCOMAS thematic conference, June 25-28, 2007, Milano, Italy, 20p.

Bouton, N., Lenain, R., Thuilot, B., & Fauroux, J.C. (2007-2). *An overturning indicator based on the prediction of the load transfer in presence of sliding: application to an All Terrain Vehicle.* In Proc. of IEEE International Conference on Robotics and Automation, ICRA'07, April 10-14, 2007, Roma, Italy, 6p., Paper 0519.pdf.

Bouton, N., *et al.* (2007-3) *A rollover indicator based on the prediction of the load transfer in presence of sliding: application to an all-terrain vehicle*. in *Intern. Conf. on Robotics and Automation (ICRA)*. Roma, Italia.

Bouton, N., et al. (2008). *A rollover indicator based on a tire stiffness backstepping observer: application to an all-terrain vehicle*. in Intern. Conf. on Intelligent Robots and Systems *(IROS)*. Nice, France.

Bouton, N., *et al.* (2009). *An active anti-rollover device based on Predictive Functional Control: Application to an All-Terrain Vehicle*.In Intern. Conf. on Robotics and Automation (ICRA). Kobe, Japan.

Bouzgarrou, B.C., Chapelle, F., & Fauroux, J.C.(2009) *Preliminary Design and Analysis of the Mobile Robot OpenWHEEL i3R*. In Proc. 3rd Third International Congress on Design and Modelling of Mechanical Systems, CMSM'09, March 16-18, 2009, Hammamet, Tunisia, ID207, 9p.

Cheek, E., et al. (2009). *Independent Suspension for Lawnmowers, Cutting Decks fnd Off-road Vehicles*. US Patent Application Publication, US 2009/0308040 A1.

Couétard, Y. (1993). *Capteur de forces à deux voies et application notamment à la mesure d'un torseur de forces*. INPI, Patent N° 96 08370 (France), 1993.

Couétard, Y. (2000). *Caractérisation et étalonnage de dynamomètres à six composantes pour torseur associé à un système de forces.* PHD Thesis, Université Bordeaux 1.

Cox, C., et al. (2009). *Methods and Apparatus for Position Sensitive Suspension Damping*. US Patent Application Publication, US 2009/0277734 A1.

M. Devy et al. (1995). On autonomous navigation in a natural environment. *Robotics and Autonomous Systems*, *16*, 5-16.

Diaz-Calderon, A., & Kelly, A. (2006). Development of a terrain adaptive stability prediction system for mass articulating mobile robots. *Field and service robots*. Vol. 24. Springer Verlag. 343-354.

Dixon, J. C. (1996). *Tires, Suspension and Handling*. London: Arnold.

Douarre, G. (2006). *Caractérisation du véhicule à 6 roues motrices Kokoon*. Final semester engineering project, IFMA, 70 p.

Fauroux, J.C., Charlat, S., & Limenitakis, M. (2004-1). Team design process for a 6x6 all-road wheelchair. In *Proc. International Engineering and Product Design Education Conference*, pp. 315-322, *IEPDE'2004*, Delft, The Netherlands, September 2nd - 3rd, 2004. All the draft papers of the author are downloadable at http://jc.fauroux.free.fr.

Fauroux, J.C., Charlat, S., & Limenitakis, M. (2004-2). *Conception d'un véhicule tout-terrain 6x6 pour les personnes à mobilité réduite*. In *Proc.* 3ème conférence Handicap 2004, June 17th - 18th, 2004, Paris Expo, Porte de Versailles / France, pp. 59-64.

Fauroux, J.C., Chapelle, F., & Bouzgarrou, B.C. (2006). *A New Principle for Climbing Wheeled Robots: Serpentine Climbing with the OpenWHEEL Platform*. Proc. of IEEE/RSJ Int. Conf. on Intelligent Robot and Systems, IROS'2006, Beijing, China, October 9-15, 2006, pp.3405-3410, file IROS06-553.pdf.

Fauroux, J.C., Vaslin, P., & Douarre, G. (2007-1). *Improving skid-steering on a 6x6 all-terrain vehicle: A preliminary experimental study*. In *Proc. of IFToMM 2007, The 12th World Congress in Mechanism and Machine Science*, June 17-21, 2007, Besançon, France, 6p., Paper A100.pdf.

Fauroux, J.C., Forlorou, M., Bouzgarrou, B.C., & Chapelle, F. (2007-2). *Design and Modeling of a Mobile Robot with an Optimal Obstacle-Climbing Mode*. In Proc. 2nd World Congress in Design and Modelling of Mechanical Systems, CMSM'2007, March 19-21, 2007, Monastir, Tunisia, 9p., Paper p98.pdf.

Fauroux, J.C., Bouzgarrou, B.C., & Chapelle, F. (2008). *Experimental validation of stable obstacle climbing with a four-wheel mobile robot OpenWHEEL i3R*. In Proc. 10th International Conference on Mechanisms and Mechanical Transmissions, MTM'2008, October 8-10, 2008, Timisoara, Romania, 8p.

Fauroux, J.C., Bouzgarrou, B.C., & Chapelle, F. (2009). Improving Obstacle Climbing with the Hybrid Mobile Robot OpenWHEEL i3R. *Mobile Robotics - Solutions and Challenges*, Edited by O.Tosun, H.L. Akin, M.O. Tokhi, G.S. Virk, World Scientific Publishing, ISBN-13 978-981-4291-26-2, Proc. 12th International Conference on Climbing and Walking Robots, CLAWAR'09, Septembre 09-11, 2009, Istambul, Turkey, pp. 765-772.

Fauroux, J.C., & Vaslin, P. (2010-1). Modeling, Experimenting, and Improving Skid Steering on a 6×6 All-Terrain Mobile Platform. *Journal of Field Robotics* 27(2), 107-126, Wiley Blackwell, ISSN: 1556-4959.

Fauroux, J.C., Chapelle, F., & Bouzgarrou, B.C. (2010-2). *OpenWHEEL i3R – A new architecture for clearance performance*. Proc. of ROBOTICS 2010, International Workshop for Environment/Agriculture, Septembre 3-4, 2010, Montoldre, France, 10p.

Fauroux, J.C., Dakhlallah, J., & Bouzgarrou, B.C. (2010-3). *A New Concept of FAST Mobile Rover with Improved Stability on Rough Terrain*. In Proc. of HUDEM'2010, 8th International Advanced Robotics Programme (IARP) Workshop on Robotics and Mechanical assistance in Humanitarian De-mining and Similar risky interventions, 10-12 May, 2010, National Engineering School of Sousse, Tunisia. Paper #26, 16 p. All the draft papers of the author are downloadable at http://jc.fauroux.free.fr.

FNSS Corp. (2008). *PARS 6x6 and 8x8 Wheeled Armoured Vehicles*. Retrieved January 29, 2009, from http://www.fnss.com.tr

Foster, J.R., Ayers, P.D., Lombardi-Przybylowicz, A.M. & Simmons, K. (2006). Initial effects of light armored vehicle use on grassland vegetation at Fort Lewis, Washington. *Journal of Environmental Management*, In Press, Corrected Proof, Available online 23 March 2006.

Gaspar, P., Szaszi, I., & Bokor, J. (2005). Reconfigurable control structure to prevent the rollover of heavy vehicles. *Control Engineering Practice*, 13: p. 699-711.

Gonzales, A., et al. (2009). On the kinematic functionality of a four-bar based mechanism for guiding wheels in climbing steps and obstacles. *Mechanism and Machine Theory*, *44*, 1507-1523.

Grand, C., et al. (2004). Stability and traction optimisation of high mobility rover - application to hybrid wheel-leg rover. *International Journal of Robotics Research*, *23(10-11)*, 1041-1058.

Halconruy, T. (1995). *Les liaisons au sol*. Editions E.T.A.I. Boulogne-Billancourt, France. 200 p.

Halme, A., et al. (2003). WorkPartner: interactive human-like service robot for outdoor applications. *International Journal of Robotics Research*, *22(7-8)*, 627-640.

Hansen, J. (2010). *The NXC guide V1.2.1r2*. 2525p. Retrieved online at http://bricxcc.sourceforge.net/nbc

Hirose, S., & Takeuchi. H. (1996). *Study on Roller-Walk (Basic Characteristics and its Control)*. Proc. of the IEEE Int. Conf. on Robotics and Automation (ICRA), pp.3265-3270.

Itoh, H. , Oida, A. & Yamazaki, M. (1995). Measurement of forces acting on 4WD-4WS tractor tires during steady-state circular turning in a rice field. *Journal of Terramechanics*, 32(5):263-283, September 1995.

Kececi E.F., & Tao G. (2006). Adaptive vehicle skid control. *Mechatronics*, 16(5):291-301, June 2006.

Kikuchi, K. et al (2008). A study on a wheel-based stair-climbing robot with a hopping mechanism. *Mechanical Systems and Signal Processing*, *22*, 1316-1326.

Kreit, F. (2008). *Modélisation d'un robot à roues franchissant une bosse et étude de son comportement et de ses paramètres d'influence.* IFMA final year project.

Lacroix, S., et al. (2002). Autonomous Rover Navigation on Unknown Terrains: Functions and

Integration. *International Journal of Robotics Research*, 21(10-11), 917-942.
Lenain, R., *et al.* (2007). Adaptive and Predictive Path Tracking Control for Off-road Mobile Robots. *European Journal of Control*. **13**(4): p. 419-439.
Maclaurin B. (2006). A skid steering model with track pad flexibility. *Journal of Terramechanics*, In Press, Corrected Proof, Available online 9 June 2006.
Matschinsky, W. (1999). *Road Vehicle Suspensions*. Professional Engineering Publishing.
McIntyre, K. (2009). *Suspension Height Adjustment Mechanism*. US Patent Application Publication, US 2009/0261542 A1.
Mendonca, C., & Nait Hadi, H. (2007). *Modélisation et expérimentation du véhicule à six roues motrices Kokoon.* Master's thesis, Université Blaise Pascal. 51 p.
Michaud, F., et al. (2003). AZIMUT - A leg-track-wheel robot. Proc. Of IEEE/RSJ Int. Conf on Intelligent Robots and Systems (IROS 03), pp. 2553-2558.
Michelin. (2008). *Michelin Active Wheel , Mondial de l'Auto 2008. Pressbook.* Retrieved online in April 2010 on http://www.michelin.com.
Miège, A.J.P., & Cebon, D. (2002). Design and implementation of an active roll control system for heavy vehicles. in 6th Int. symposium on Advanced Vehicle Control (AVEC). Hiroshima, Japon.
Mokhiamar, O., & Abe, M. (2006). How the four wheels should share forces in an optimum cooperative chassis control. *Control Engineering Practice*, 14(3):295-304, March 2006.
Mousset, C.H., & Chervet, T. (2008). *Modélisation et expérimentation du véhicule à six roues motrices Kokoon.* Master's thesis, Université Blaise Pascal. 58 p.
MSC Software Inc. (2008). *Adams 2008 software documentation on CD-ROM*. Chapters “Contact” and “Impact”.
Nakajima, S., et al. (2004). *Motion Control Technique for Practical Use of a Leg-Wheel Robot on Unknown Outdoor Rough Terrains*. Proc. of IEEE/RSJ Int. Conf. on Intelligent Robots and Systems (IROS 04), pp.1353-1358.
National Highway Traffic Safety Administration (NHTSA). (2005). *Trends in static stability factor of passengers cars, light trucks and vans*. U.S. department of transportation: Springfield, U.S.A.
Oasis LLC Corp. (2009). *The Max 6x6 ATV*. Retrieved January 29, 2009, from http://www.oasisllc.com/english/max.htm
Pacejka H.B. (2006). *Tire and Vehicle Dynamics*. SAE Edition, Warrendale, USA. Second edition. 642 p.
Papadopoulos, E.G., & Rey, D.A. (1996). *A new measure of tipover stability margin for mobile manipulators*. in *Inetrn. Conf. on Robotics and Automation*. Minneapolis, U.S.A.
Patria Corp. (2009). *The Armoured Modular Vehicle*. Retrieved January 29, 2009, from http://www.patria.fi.
Reimpell J. (2001). *The Automotive Chassis: Engineering Principles*. Elsevier ISBN 0 7506 5054 0.
Richalet, J. (1993). *Pratique de la commande prédictive*. Hermes. 349p.
Richalet, J., et al. (1997). *Predictive functional control - application to fast and accurate robots*. In 10th IFAC World Congress. 1997. Munich, Germany.
Robosoft Corp. (2009). *The Pioneer 3 ATRV*. Retrieved January 29, 2009, from http://www.robosoft.fr.
Rollins, E., et al. (1998). *Nomad: A Demonstration of the Transforming Chassis*. Proc. of Intelligent Components for Vehicles (ICV 98), Spain.
Sacli M. (2009). *Suspension System Providing Two Degrees of Freedom*. PCT patent WO 2009126787.
Sardain, P., & Bessonet, G. (2004). *Forces acting on a biped robot. Center of pressure - Zero moment point.* IEEE Transactions on systems, man, and cybernetics.**34**(5): p. 630-637.
Schofield, B., Hagglund, T., & Rantzer, A. (2006). *Vehicle dynamics control and controller allocation for rollover prevention*. in International conference on control applications. Munich, Germany.
Shoichi S., Yoshimi F. & Yutaka T. (1986). *Steering apparatus for a vehicle having steerable front and rear wheels*. Patent number US4614351, 1986-09-30, Honda Motor Co Ltd (Japan).
Siegwart, R., & Nourbakhsh, I.R. (2004). *Introduction to autonomous mobile robots.* MIT Press.
Sreenivasan, S.V., & Wilcox, B.H. (1994). Stability and traction control of an actively actuated micro-rover. *Journal of Robotic Systems*, 11(6):487-502, September 1994.
Stéphant, J. (2004). Contribution à l'étude et à la validation expérimentale d'observateurs appliqués à la

dynamique du véhicule. In *Technologie de l'information et des systèmes*. Université de Technologie de Compiègne (UTC): Compiègne, France. p. 312.

Vivas, A., & Mosquera, V. (2005). *Predictive functional control of a {PUMA} robot*. in Proc. of the first ICGST International Conference on Automatic Control and Systems Engineering (ACSE). Cairo, Egypt.

Watanabe, K., Kitano, M., & Fugishima, A. (1995). Handling and stability performance of four-track steering vehicles. *Journal of Terramechanics*, 32(6):285-302, November 1995.

Wong J.Y. (2008). *Theory of ground vehicles. John Wiley* & Sons, Hoboken, New Jersey, USA. Fourth edition. 592p.

ADDITIONAL READING SECTION

Alexander, R. (2006). *Principles of Animal Locomotion*. Princeton University Press. 384p.

Behn, C., Zeidis, I., & Zimmermann, K. (2009). *Mechanics of Terrestrial Locomotion: With a Focus on Non-pedal Motion Systems*, Springer-Verlag Berlin Heidelberg. 277p.

Gonzalez de Santos, P., Garcia E., Estremera, J. (2006). *Quadrupedal Locomotion, An Introduction to the Control of Four-legged Robots*, Springer-Verlag London. 267 p.

Milliken, W.F., & Milliken, D.L. (1995). *Race Car Vehicle Dynamics*. Society of Automotive Engineers Inc. 1000p.

Muybridge, E. (1957). Animals in Motion. Dover Publications. 1st edition (June 1, 1957).416 p.

Ridderström,C. (2003). *Legged locomotion: Balance, control and tools - From equation to action*, PHD thesis, Department of Machine Design, Royal Institute of Technology, Stockholm, Sweden, 2003, 266p.

Wong, J.Y. (2009). *Terramechanics and Off-Road Vehicle Engineering, Second Edition: Terrain Behaviour, Off-Road Vehicle Performance and Design*. Butterworth-Heinemann. 488p.

KEY TERMS & DEFINITIONS

- Backstepping observer: observer dedicated to grip conditions estimation.
- Hybrid locomotion: a general term to describe locomotion using combinations of classical locomotion systems such as wheels, legs or tracks.
- Lateral dynamic stability: dynamic stability of the vehicle during a curve.
- Lateral Load Transfer: stability criterion based on the normal forces exerted on each wheel of the vehicle.
- Light all-terrain vehicles: vehicles designed to move on natural ground, essentially used in agricultural area (as quad bikes)
- Predictive control: Advanced control law used to control a system by predicting its next future.
- Off-road mobile robot: robots designed to move on irregular ground.